Title: **Akt regulates axon wrapping and myelin sheath thickness in the PNS**

Abbreviated title: Akt regulates PNS axon wrapping and myelination

Enric Domènech-Estévez[1,2,3,§,*], Hasna Baloui[1,2,3,§], Xiaosong Meng[1,2], Yanqing Zhang[1,2], Katrin Deinhardt[4], Jeff L. Dupree[5], Steven Einheber[6] , Roman Chrast[3], James L. Salzer[1,2,*]

[1] Neuroscience Institute and [2] Departments of Neuroscience and Physiology and Neurology, NYU-Langone Medical Center, New York, NY 10016 USA

[3] Department of Neuroscience and Department of Clinical Neuroscience, Karolinska Institutet, 17177 Stockholm, Sweden

[4] Centre for Biological Sciences, Faculty of Natural & Environmental Sciences, University of Southampton, Southampton, SO17 1BJ, UK

[5] Department of Anatomy and Neurobiology, Virginia Commonwealth University Medical Campus, Box 980709, Richmond, VA 23298-0709, USA

[6] Department of Medical Laboratory Sciences, Hunter College, CUNY, New York, NY 10010, USA

[§] Those authors contributed equally to the work

*** Corresponding Authors:** Enric Domènech-Estévez, PhD, Retzius väg 8, 17177 Stockholm, Sweden +46852486542 enric.domenech-estevez@ki.se, and James L. Salzer, MD, PhD, 550 First Avenue, New York, NY, 10016 USA +12122630758 james.salzer@nyumc.org.

Number of pages: 38

Number of figures: 9

Number of words: Abstract (250), Introduction (614), Discussion (1618).

Conflicts of interest: The authors declare no competing financial or any other conflict of interests.

Acknowledgements: This work was supported by NIH grant NS26001 (JLS) and the NYU Cancer Institute Center support Grant NIH/NCI 5P30CA16087-31. EDE was partially funded by the Spanish Ministerio de Educación y Ciencia-Fulbright commission. EDE, HB and RC are supported by Strategic Research Area Neuroscience (StratNeuro) program. We thank Eric Roth and Feng-Xia Liang (NYU) and Kjell Hultenby and Eva Idsund (KI) for assistance with EM of mouse neural tissue, and Dr. Teresa Milner (Weill Cornell Medical College) for assistance with EM of the cocultures. We thank Dr. Frédéric Schütz (University of Lausanne) for his support with statistics.

ABSTRACT: The signaling pathways that regulate myelination in the peripheral nervous system (PNS) remain poorly understood. Phosphatidylinositol-4,5-bisphosphate 3-kinase 1A (PI3K), activated in Schwann cells by neuregulin and the extracellular matrix, has an essential role in the early events of myelination. Akt/PKB, a key effector of PI3K, was previously implicated in CNS, but not PNS myelination. Here we demonstrate that Akt plays a crucial role in axon ensheathment and in the regulation of myelin sheath thickness in the PNS. Pharmacological inhibition of Akt in DRG neuron-Schwann cell cocultures dramatically decreased MBP and P0 levels and myelin sheath formation without affecting expression of Krox20/Egr2, a key transcriptional regulator of myelination. Conversely, expression of an activated form of Akt in purified Schwann cells increased expression of myelin proteins, but not Krox20/Egr2, and the levels of activated Rac1. Transgenic mice expressing a membrane-targeted, activated form of Akt under control of the 2',3'-cyclic nucleotide 3'-phosphodiesterase (CNP) promoter, exhibited thicker PNS and CNS myelin sheaths, and PNS myelin abnormalities such as tomacula and myelin in/outfoldings centered around the paranodes and Schmidt Lanterman incisures. These effects were corrected by rapamycin treatment *in vivo*. Importantly, Akt activity in the transgenic mice did not induce myelination of non-myelinating

Schwann cells in the sympathetic trunk or Remak fibers of the dorsal roots although, in those structures, they wrapped membranes redundantly around axons. Together, our data indicate that Akt is crucial for PNS myelination driving axonal wrapping by unmyelinated and myelinated Schwann cells and enhancing myelin protein synthesis in myelinating Schwann cells.

Key words: Akt; Schwann cell; myelin; transgenic; wrapping; mTOR

SIGNIFICANCE STATEMENT: Although the role of the key serine/threonine kinase Akt in promoting CNS myelination has been demonstrated, its role in the PNS has not been established and remains uncertain. This work reveals that Akt controls several key steps of the PNS myelination. Firstly, its activity promotes membrane production and axonal wrapping independent of a transcriptional effect. In myelinated axons, it also enhances myelin thickness through the mTOR pathway. Finally, sustained Akt activation in Schwann cells leads to hyper/dysmyelination, mimicking some features present in neuropathies, such as Hereditary Neuropathy with Liability to Pressure Palsies or demyelinating forms of Charcot-Marie-Tooth disease. Together, these data demonstrate the role of Akt in regulatory mechanisms underlying axonal wrapping and myelination in the PNS.

INTRODUCTION

Formation of the myelin sheath in the PNS is among the most dramatic examples of axon-glial interactions (Mirsky et al., 2008). Schwann cells are intimately associated with axons and adopt distinct fates as either myelinating or non-myelinating, i.e. Remak Schwann cells. These two Schwann cell phenotypes are distinguished by both their morphological relationship with the axon and by different transcriptional profiles. A number of axonal signals have been implicated in the regulation of the Schwann cell phenotype, including ADAM22 which binds Lgi4 secreted by the Schwann cell and the axonal growth factor neuregulin1 type III (Nrg1III), which activates the ErbB2/ErbB3 heterodimer on Schwann cells (see (Kidd et al., 2013; Nave and Werner, 2014; Monk et al., 2015; Salzer, 2015) for recent reviews).

Nrg1, in particular, controls virtually all aspects of the Schwann cell lineage including initial gliogenesis, proliferation, ensheathment and myelination of axons. High levels of Nrg1III on the axonal membrane provide a threshold signal for the induction of myelination and regulate the thickness of the myelin sheath (Michailov et al., 2004; Taveggia et al., 2005; Nave and Salzer, 2006). Nrg1III activates the Mitogen-activated protein kinase (MAPK), Phosphatidylinositol 3-kinase 1A (PI3K) and Phospholipase C gamma (PLCγ) pathways, each of which has been implicated as essential for proper myelination (Newbern and Birchmeier, 2010). The precise roles of these signaling pathways in the transcriptional and morphogenetic events of myelination however, remain to be established.

Previous studies using *in vitro* models demonstrated that PI3K activation is necessary for proper PNS myelination (Maurel and Salzer, 2000; Ogata et al., 2004). A promyelinating role of PI3K was further supported by studies in mice in which the Phosphatase and tensin homolog (PTEN), a PI-3 phosphatase, was conditionally inactivated in glia thereby driving sustained activation of PI3K (Goebbels et al., 2010). Loss of PTEN function in these mice, as well as inactivation of its interactor Dlg1 (Cotter et al., 2010; Goebbels et al., 2010; Noseda et

al., 2013) results in PNS hypermyelination and increased wrapping of small caliber axons by Schwann cells.

The serine/threonine kinase Akt has been thought to be the major PI3K effector during myelination, particularly in the CNS (Flores et al., 2008). Mice expressing a constitutively active, phospho-mimetic form of Akt under control of the proteolipid protein (PLP) promoter, exhibit hypermyelination in the CNS. Surprisingly the PNS of these mice was not hypermyelinated (Flores et al., 2008) leaving open the question of the role of Akt in Schwann cells.

Here we use loss and gain of function approaches to provide direct evidence that Akt promotes PNS myelination and axonal wrapping. Pharmacological inhibition of Akt activity abrogates myelin formation *in vitro*, without affecting the levels of Krox20/Egr2, a transcription factor crucial for PNS myelination (Zorick et al., 1996; Decker et al., 2006). Conversely, mice that express a myristoylated, constitutively active Akt transgene in myelinating glia under control of the 2',3'-cyclic nucleotide 3'-phosphodiesterase (CNP) promoter, exhibit hypermyelination in the PNS and CNS. No conversion of axons from an unmyelinated to a myelinated fate was observed in these mice, although aberrantly, hyperwrapped Remak fibers are common. These mice also exhibit focal hypermyelination, a pathological hallmark of some models of peripheral neuropathies (Adlkofer et al., 1997; Bolino et al., 2004; Tersar et al., 2007; Robinson et al., 2008). They develop myelin defects similar to those described in a model of tomaculous neuropathy (Goebbels et al., 2012), which can be corrected with rapamycin treatment. Finally, Akt activation *in vitro* results in activation of Rac1, previously implicated in myelin sheath wrapping (Thurnherr et al., 2006; Benninger et al., 2007; Nodari et al., 2007).

Together, these data indicate that Akt promotes Schwann cell wrapping and myelination via multiple distinct pathways involving mTOR and Rac1 activation.

MATERIAL AND METHODS

Generation of the CNP-MyrAkt and CNP-AktDD transgenic mice:

cDNAs for MyrAktHA and HAAktDD were kindly provided by Dr. Thomas Franke (New York University) (Franke et al., 1995; Matsui et al., 1999). A plasmid containing the CNP promoter (Gravel et al., 1998) was kindly provided by Dr. Karen Chandross (Sanofi).

CNP-MyrAkt: The vector containing the CNP cassette was digested with BamHI and dephosphorylated with CIP phosphatase. MyrAktHA was released using BamHI/BglII digestion and inserted after the CNP promoter. The construct CNP-MyrAktHA was then released by sequential digestion AseI/BtsI. DNA was purified by gel extraction (QIAquick gel extraction, Qiagen), salt elution (Elutip-D, Whatman #10462615), and ethanol precipitation.

CNP-AktDD: The vector containing the CNP cassette was digested with AfeI/BamHI. An initial ClaI digestion followed by Kleenow filling was done in AktDD cDNA. Afterwards, BamHI digestion was performed. The insert was ligated after the CNP promoter and then released using AseI/MluI digestion. The DNA was purified as described for the CNP-MyrAktHA construct.

The constructs were injected into FVB females in the NYUMC Transgenic Mouse Core. Positive founders were PCR identified over tail DNA using the primers TgAktFd (5'-TCT GAG GAT GCC AAG GAG AT-3') and TgAktRev (5'-GGG CGA TCG AGT GAA TTG TA-3'). To ensure the specificity of the PCR product, one of the primers was designed to match a portion of plasmid inserted with the cassette. Founders were backcrossed to C57Bl6 wild-type mice for at least five generations before analysis; sibling littermates were used in all analyses. All experiments were carried out with the L1MyrAkt line, but a similar phenotype was observed in the L2MyrAkt line. In some cases (AktDD), analysis was done on founders because of infertility. All experiments with mice were performed in accordance with the legal requirements of NYU.

143 *Akt knockouts*: Akt1KO (Cho et al., 2001a) and Akt2KO (Cho et al., 2001b) were
144 obtained from The Jackson Laboratory (stock numbers 004912 and 006966, respectively).
145 Akt3KO (Easton et al., 2005) were obtained from Dr. Morris J. Birnbaum (University of
146 Pennsylvania) under MTA agreement.

147 *Materials.* Antibodies to specific proteins were obtained from the following companies:
148 Cell Signaling Technology (total Akt1-3, pAkt Ser473, pAkt Thr308, total c-Jun and p c-Jun
149 Ser73, total S6RP and pS6RP Ser235/236, total GSK3b and pGSK3b Ser9, rabbit HA),
150 Millipore (rabbit MBP, chicken P0, chicken MBP, mouse NeuN); Covance (mouse SMI 94 MBP,
151 chicken Neurofilament), Sigma (mouse tubulin, rabbit anti-EHS laminin, rabbit actin, mouse
152 HA.11). Rabbit anti-Krox20 and rabbit anti-Oct6 were kindly provided by Dr. Dies Mejer
153 (University of Edinburg), guinea pig anti-CASPR by Dr. M. Bhat (University of North Carolina)
154 and guinea pig anti-Oct6 antibody was provided by Dr. Jeremy Dasen (New York University).
155 Secondary antibodies conjugated to rhodamine, AMCA or Alexa 488 were obtained from
156 Jackson ImmunoResearch.

157 *Immunoblotting.* Tissues were lysed in 2% SDS, 25 mM Tris, 95 mM NaCl and 10 mM
158 EDTA buffer with protease inhibitors (complete Mini EDTA-free tablets, Roche 11836170001)
159 and phosphatase inhibitors (PhosSTOP, Roche 04906837001). Nerves were sonicated 10
160 seconds at the lowest intensity. Fifteen to fifty micrograms of protein was loaded on 12.5%
161 SDS-PAGE gel. After transfer on nitrocellulose membrane (Whatman #10402580), and
162 incubation with primary antibodies, the blots were developed and quantified by using infrared
163 secondary antibodies and software from Odyssey Imager (LI-COR Biosciences).

164 *Lentivirus production and infection*: Doxycycline inducible lentiviruses were created in
165 the pSLIK-Hygromycin vector as per the manufacturer's instructions (Invitrogen, Gateway
166 Technology with clonase II). Confluent 293FT cells were lipofected with LipoD293 reagent
167 (SignaGen laboratories SL 100668). A triple lipofection with Δ8.9 (4 μg), VSVG (6 μg) and

MyrAkt-HA or green fluorescent protein (GFP) (5 µg) was performed. Supernatant was collected 48 hours after lipofection and used to infect Schwann cells. Infected cells were selected for 9 days with 200 µg/ml of hygromycin (Hygrogold, Invivogen # ant-hg-1) prior to use in experiments. Induction was performed by adding doxycycline (2 µg/ml) to the culture media for four days.

Dorsal root ganglia neuron-Schwann cell cocultures: Rat neuron-Schwann cell cocultures were performed as previously described (Taveggia et al., 2005).

Rapamycin and LY294002 (LY) were obtained from LC Laboratories (R-5000 and L-7962 respectively). Perifosine (Pf) was obtained from Cayman Chemical Company (10008112). Drugs (20 µM of LY294002 or 20 µM of perifosine) were added 24 hours prior to and then continued after switching the cocultures to myelinating media.

Rac1 and cdc42 pull down: Schwann cells were infected with inducible MyrAkt and processed as described above. Doxycycline was then added to the proliferative Schwann cell media for 4 days and Rac1 and cdc42 activities were analyzed as previously described (Deinhardt et al., 2011). To generate the respective plots, values of active GTPase levels were divided by the total GTPase levels after actin normalization, which was used as a loading control.

Cell culture immunofluorescence and immunohistochemistry: Mice were fixed via transcardial perfusion with 4% PFA. Dissected brains were postfixed in 4% PFA overnight at 4° C, cryoprotected by immersion in 20% sucrose in PBS. 40 µm floating sections were prepared on a cryostat. Cells were fixed 15 minutes with 4% PFA. Tissue and cells were processed for immunostaining as previously described (Zanazzi et al., 2001). For Fig. 4*D*, adult mouse sciatic nerve and dorsal root ganglia were fixed in 1% PFA and embedded for cryosectioning and processed for immunofluorescence.

Teased fibers: Sciatic nerves were harvested from six-months old animals and fixed in 2% PFA for four hours. After a 10 minute wash in 30 mM glycine PBS, the fibers were teased on a glass slide using needles, and dried overnight. Slides were kept at -80º C until needed. Tissue was permeabilized 20 minutes in cold methanol prior to staining as described above. Then, the same protocol as used for cell staining was followed.

Proliferation assay: 50,000 rat Schwann cells were seeded into established, purified rat neuron cultures for 24h prior to adding the drugs (Pf and LY) to the media in a final volume of 400 µl. Twenty hours later, cocultures were exposed to media containing the drugs and 20 µM of bromodeoxyuridine (BrdU) for 4 hours. Cells were then fixed in PFA 4%, permeabilized with methanol and treated as previously described (Maurel and Salzer, 2000). The ratio of BrdU positive:Hoechst positive cells were calculated from non-overlapping pictures of the whole coverslip. Four independent sets of experiments were performed (n=4), and from each of them, three independent coverslips were screened.

RNA extraction and quantitative real-time PCR: Total RNA was isolated using a RiboPure Kit (Ambion). cDNA was generated from 250-600 ng of total RNA by AMV Reverse Transcriptase (Promega) and the transcripts were detected and amplified by quantitative real-time PCR in a LightCycler machine (Roche) following the manufacturer's instructions. GAPDH was used as internal control. Real-time PCR conditions were as follows: 1 cycle 10' 95º C, 50 cycles (30'' 95º C, 30'' 56º C, 30'' 72º C), 1 cycle 1' 95º C, 30'' 55º C and 30'' 95º C. Primers: *MAG* Fd 5'-ACC TTG CAG TTC GAG GGT TA-3', *MAG* Rev 5'-ACA GAG CAG GCT GAC ATG G-3'; *MBP* Fd 5'-ACT ACC CAC TAC GGC TCC CT-3', *MBP* Rev 5'-GGG TGT ACG AGG TGT CAC AA -3'; *Krox20* Fd 5'-GGT GTG TGT ACC ATG TCC CA-3', *Krox20* Rev 5'-CCA GAG AGG AGG TGG AAG TG-3'; *GAPDH* Fd 5'-AGA AGA CTG TGG ATG GCC C-3'; *GAPDH* Rev 5'-TTC AGC TCT GGG ATG ACC TT-3'; *MPZ* Fd 5'-TCC CTC ATC CAG CCC CAG CC-3', *MPZ* Rev 5'-CTG GGA GCG CAC AGC ACC AT-3'.

Rapamycin treatment in vivo: The drug was dissolved in vehicle solution containing 5% polyethylene glycol 400, 5% Tween 80, and 8% ethanol. Rapamycin (7.5 mg/kg) or vehicle was administered intraperitoneally for 5 days a week during 8 weeks. Mice were treated beginning at 5 weeks of age and were weighed every week to adjust the treatment. A total of 21 mice were treated, 7 WT and 7 Tg with vehicle, and 7 Tg with rapamycin. Two independent rounds of treatment were done for morphometric and WB analyses.

Electronic microscopy and morphometric analysis: Control and treated three weeks old myelinating cocultures grown on collagen-coated glass coverslips were rinsed in PBS and fixed overnight at 4° C in 2% glutaraldehyde in 0.1 M phosphate buffer pH 7.0 (0.1 M PB). After gently removing the fixed cultures from the coverslips they were washed in 0.1 M PB, incubated in 2% osmium tetroxide in 0.1 M PB for 1 hour and processed for flat embedding in EMbed 812 (Electron Microscopy Sciences, Fort Washington, PA). Ultrathin sections were counterstained with uranyl acetate and Reynold's lead citrate and examined on a Philips (Eindhoven, The Netherlands) CM10 electron microscope. For the *in vivo* analysis, mice were fixed via transcardial perfusion with 4% paraformaldehyde, 2.5% glutaraldehyde and 0.1 M sucrose in 0.1 M PB, pH7.4. Sciatic nerves, spinal roots (L4 level), optic nerve and sympathetic tract were collected. Tissues embedded in EMbed 812 were sectioned on a Leica UCT ultramicrotome at a thickness of 1 µm and stained with a solution of 1% toluidine blue. For TEM, tissues embedded in EMbed 812 were sectioned on a Leica UC6 ultramicrotome at a thickness of 90 nm and placed on copper slotted grids or occasionally on mesh grids. Sections were stained with 3% uranyl acetate in 50% methanol for 20 minutes followed by lead citrate for 5 minutes. Grids were viewed on a Philips CM12 Tungsten Emission TEM at 120kV and imaged with a GATAN 4k x 2.7k digital camera.

For g-ratios, non-overlapping digitized images of fiber cross-sections from dorsal roots were obtained and analyzed using Nikon software. G ratio were calculated by dividing the axon

diameter by the total fiber diameter. G ratios were determined exclusively in the dorsal root due to their mix of small and large caliber axons. All fibers with myelin abnormalities or fixation artifacts were excluded from analysis. Three animals per genotype were used for the WT/MyrAkt data (Fig. 5*D, E*), and four animals per genotype and conditions were quantified for the rapamycin experiments (Fig. 9*D*). The number of axons per Remak bundle and the number of axons in Schwann cell pockets were counted in the sciatic nerve by using Image J software (National Institute of Health). The number of axons per 100 μm^2 and the total number of myelin abnormalities per sciatic nerve were determined from merged micrographs of thin sciatic nerve sections (400X), assembled with Adobe Photoshop (Fig. 9*C*). Overlapping digitized images (400X) from thin sections of dorsal and ventral roots were merged to determine the total number of myelinated axons in Fig. 6*F*.

Statistical analysis: The unpaired two-tailed T-test was performed on all data to assess significance. In each case, the standard error of the mean (SEM) is shown in the plots although only the upper part of the SEM is depicted. Each n represents a different independent experiment or animal. Significance was considered for $p < 0.05$ (*) and $p < 0.01$ (**).

RESULTS

Akt activity is required for myelination and axon sorting

To address a role of Akt in myelination, we first examined Akt null mice for any abnormalities in the peripheral nerves. There are three Akt genes (Akt1, Akt2 and Akt3), each with different tissue expression and substrate affinities (Easton et al., 2005; Tschopp et al., 2005; Franke, 2008; Leavens et al., 2009). Western blot analysis revealed that Akt1 is expressed in both neurons and Schwann cells whereas Akt2 and Akt3 are primarily expressed by Schwann cells and neurons, respectively (Fig. 1*A*). We next examined whether mice deficient in each of these Akt isoforms exhibit myelination defects by comparing sciatic nerves

from two month-old WT vs. knockout mice via semithin sections. There were no obvious differences between the knockout mice and their wild type littermates in terms of nerve size or the extent of myelination (Fig. 1*B*). No obvious abnormalities of myelinated fibers or Remak bundles were evident on inspection of electron micrographs of the Akt mutants vs. their WT littermates (Fig. 1*B*a-f). The overall preservation of morphology in individual mutants likely reflects compensation by remaining Akt isoforms.

We therefore undertook to inhibit all Akt activity with the pharmacological inhibitor perifosine (Pf), an alkylphospholipid that impairs Akt by blocking its PH domain (Hennessy et al., 2007; Gills and Dennis, 2009). In parallel, we inhibited PI3K activity with the LY294002 (LY) inhibitor (Vlahos et al., 1994; Maurel and Salzer, 2000). Treatment of cocultures with each inhibitor blocked nearly all myelin formation (Fig. 2*A*, *B*). In agreement, expression levels of MBP and P0 protein (Fig. 2*C, D*) were significantly reduced in the Pf-treated and nearly absent in the LY-treated cocultures. mRNA levels for MBP were dramatically reduced in the presence of either drug whereas the effect of Pf on P0 was more modest, perhaps due to its higher basal levels of expression (Fig. 2*E*). Unexpectedly, Oct6/SCIP and Krox20, key transcription factors for PNS myelination, were robustly expressed in the nuclei of the Pf-treated Schwann cells (Fig. 2*A*) and the levels of Krox20 protein (Fig. 2*C*, *D*) and mRNA (Fig. 2*E*) were unaffected. These results suggest that the promyelinating effects of Akt are independent of Krox20. In contrast to Pf, cocultures treated with LY did not express any Krox20 protein or mRNA (Fig. 2*A, C*-*E*).

There was no effect of Pf on Schwann cell proliferation in the cocultures (Fig. 2*F*), in further contrast to LY (Fig. 2*F*), which is known to inhibit Schwann cell proliferation induced by axonal neuregulin (Maurel and Salzer, 2000). Consequently Schwann cell numbers were markedly reduced in the LY- but not the Pf-treated cocultures (Fig. 2*A*). To determine whether reduced numbers of Schwann cells in the LY treated cocultures contributed to the limited

expression of Krox20, we seeded a 5 fold excess of SCs prior to treatment with LY. No significant Krox20 or myelin protein expression was detected under these conditions (data not shown) indicating that the effects of LY are independent of an effect on cell numbers.

Our results confirm that PI3K activity is crucial for myelination *in vitro* and reveal that its effector Akt controls myelin mRNA and protein expression in the PNS, independent of Krox20 regulation. The data also suggests that PI3K regulates Schwann cell proliferation and the expression of myelin transcription factors by mechanisms independent of Akt.

Ultrastructural analysis of these cultures further revealed that Pf and LY differentially affected Schwann cell ensheathment. Schwann cells in the Pf-treated cultures partially surrounded the axons, although did not completely wrap most of them (Fig. 2*G*). In contrast, in the LY treated cocultures, Schwann cell were apposed to but completely failed to ensheathe axons (Fig. 2*G*). Myelination was dramatically reduced by both treatments.

Activated Akt enhances myelin protein and mRNA expression *in vitro* independent of Krox20 levels

We next examined whether Akt activity is not only necessary, but is also sufficient for triggering myelination. We used a lentiviral vector to express a doxycycline-inducible, HA-tagged myristoylated Akt (MyrAkt) in cultured Schwann cells. MyrAkt is expressed and active at the membrane independent of PIP3 concentrations. After infection, Schwann cell cultures were maintained on media containing ascorbate in the presence or absence of doxycycline for four days. Schwann cells infected with a doxycycline-inducible lentivirus encoding GFP, which served as a control, displayed no increase of myelin proteins or Krox20 (Fig. 3*A*). In general, the expression of activated Akt increased MAG and P0 protein and mRNA levels; this increase was significant in the case of MAG protein (Fig. 3*B-D*). Interestingly, Krox20 protein levels were slightly reduced and mRNA levels unchanged despite the induction of myelin proteins following

316 MyrAkt expression (Fig. 3*B-D*) suggesting these changes were independent of Krox20
317 regulation.
318
319 **Transgenic expression of activated Akt isoforms results in PNS hypermyelination**
320 To assess the role of Akt *in vivo*, we generated transgenic mice expressing HA-tagged
321 MyrAkt or AktDD in myelinating glia under control of 2', 3'-cyclic nucleotide 3'-
322 phosphodiesterase (CNP) promoter elements (Fig. 4*A*). Both Akt1 isoforms are constitutively
323 active as the result of either being targeting to the membrane (MyrAkt) or via mutations of two
324 phosphorylation sites (Thr308 and Ser473) to aspartate that mimic the activated state (AktDD)
325 (Fig. 4*A*). We generated four CNP-MyrAkt positive founders and three transgenic CNP-AktDD
326 founders. All four CNP-MyrAkt lines exhibited enlarged brains, optic and sciatic nerves; this
327 was evident at several months of age and quite pronounced at one year of age (Fig. 4*C*). Due
328 to breeding problems with the CNP-AktDD mice, only founders were analyzed. Only one of the
329 CNP-AktDD founder mice exhibited a hypermyelinated phenotype, evident in the sciatic nerves
330 (Fig. 5*B*).
331 Two of the CNP-MyrAkt that transmitted the transgene were analyzed in detail. In each
332 case, transgenic mice were phenotypically indistinguishable from wild type littermates until
333 approximately one year of age when they developed limited motility and breathing difficulties. In
334 agreement with the expression of CNP (Chandross et al., 1999), the HA-tagged transgene was
335 detected in transgenic sciatic nerves at P0.5, the earliest time point examined (Fig. 4*B*). Its
336 expression increased during active myelination (P10 to P21) and remained robust into
337 adulthood. Expression of the HA-tag was also detectable in DRGs directly isolated from E13.5
338 embryos (Fig. 4*B*), likely reflecting the presence of glial/satellite cells in these DRGs. In
339 agreement, staining of adult DRGs and sciatic nerves was largely if not exclusively confined to
340 glial cells (Fig. 4*D*).

Transgenic mice were hypermyelinated in both the CNS and PNS. CNS hypermyelination was evident by increased MBP staining on coronal sections and an increase in the size of the corpus callosum (Fig. 4*E*). Both the sciatic and optic nerves were also markedly expanded in diameter, based on toluidine blue staining of semi-thin sections (Fig. 5*A*). Electron micrographs showed that individual nerve fibers were hypermyelinated (Fig. 5*B*) evident as an increase in the number of myelin lamellae; myelin periodicity was unaffected (Fig. 5*C*). G-ratios were significantly decreased in 5 month-old transgenic mice (Figs. 5*D*, *E*). Hypermyelination was most pronounced in small caliber axons, i.e. those less than 2 microns in diameter in both the dorsal roots (Fig. 5*D*, *E*) and ventral roots (data not shown).

The total numbers of Hoechst positive cells in the ventral and dorsal roots were counted. No significant differences in cell numbers were detected in four transgenic roots as compared to roots from their WT littermates (Fig. 5*F*). These results suggest that in our system, tissue hypertrophy results from an Akt-mediated increase in myelin and, perhaps, increased extracellular matrix production, rather than increased numbers of cells.

Akt activation promotes Schwann cell wrapping but does not alter the ensheathment fate of axons

Remak fibers were also affected in the CNP-MyrAkt transgenic mice. In wild type nerves as expected, small caliber axons were enclosed within individual pockets of a single unmyelinated Schwann cell (Fig. 6*A*). In contrast, in the transgenic nerves, multiple layers of Schwann cell membrane frequently wrapped small caliber axons. High power micrographs revealed these wrapped membranes were non-compacted (inset in 6*A*, middle panel); pockets with a normal structure that enclosed axons were absent (Fig. 6*A*I). Transgenic Schwann cell pockets sometimes contained collagen fibers rather than axons; these were more frequent in older animals and were surrounded by basal lamina (Fig. 6*A*II). Indeed, Schwann cell

processes were also seen surrounded by basal lamina without any axonal contact suggesting that Akt can drive Schwann cell basal lamina formation in the absence of axonal signals (Fig. 6*B*I). Some pockets were formed even without any detectable content (Fig. 6*B*II) and, in such cases, a reversed orientation of the basal lamina was detected, secreted inside the empty pocket (Fig. 6*B*II). Finally, there was a trend to enhanced segregation of unmyelinated axons. This was evidenced by an increase in transgenic Remak bundles that enclosed just one to five axons (quantified in Fig. 6*C*) or with single-axon pockets (Fig. 6*D*) compared to WT bundles.

We also asked whether Akt activation is sufficient to convert unmyelinated, post-ganglionic sympathetic nerve fibers to a myelinated fate, akin to the effects of overexpressing Nrg1III in these axons (Taveggia et al., 2005). Examination of the sympathetic tract of transgenic mice (Fig. 6*E*) revealed that fibers were consistently unmyelinated. Instead, multiple layers of Schwann cell membrane surrounded the axons thus resembling the Remak bundles in the sciatic nerves and dorsal roots of the transgenic mice. Schwann cell pockets containing only extracellular matrix were also found in this tract (Fig. 6*E*).

In agreement with a lack of effect on myelination, the proportion of myelinated fibers in the dorsal and ventral roots of transgenic and wild type mice were comparable (Fig. 6*F*). Together, these data suggest that Akt regulates axonal wrapping and that other signals are required for myelination.

MyrAkt specifically enhances Rac1 activity in Schwann cells

Rac1 and cdc42 are crucial for proper sorting of axons at early stages of myelination; their precise roles differ as cdc42 controls the pool of Schwann cells by affecting proliferation whereas Rac1 induces radial lamellopodia required to sort axons (Benninger et al., 2007; Nodari et al., 2007). To assess whether the enhanced axonal sorting and wrapping observed in MyrAkt animals might reflect activation of Rac1 or cdc42, we induced MyrAkt in cultured

Schwann cells. Induction of Akt led to activation of Rac1 but not cdc42 based on pull-downs with GST-Pak1 (Fig. 7*A, B*); there was no change in total levels of either Rac1 or cdc42. This data suggests that part of the phenotype observed in the transgenic mice, such as enhanced Schwann cell sorting, is a consequence of increased Rac1 activity.

Transgenic nerves develop tomacula and myelin outfoldings/infoldings

A consistent finding in the MyrAkt sciatic nerves was the presence of numerous myelin abnormalities. These included myelin outfoldings, a histological hallmark of some Charcot-Marie-Tooth (CMT) forms, notably CMT4B (Bolis et al., 2005; Tersar et al., 2007), and tomacula, i.e. focal thickenings of the myelin sheath characteristic of Hereditary Neuropathy with Liability to Pressure Palsies (HNPP) (Adlkofer et al., 1997); tomacula were also seen in the PTEN conditional knockout mice (Goebbels et al., 2012). Five month-old nerves developed mostly myelin infoldings (Fig. 8*A*, left panel, and Fig. 8*B*II) and tomacula (Fig. 8*A*, right panel, and Fig. 8*B*I). These changes were preferentially located to regions of non-compacted myelin, i.e. the paranodes and Schmidt-Lanterman incisures. Tomacula were accompanied by axonal compression at the affected regions, although no axonal degeneration was detected at the ages examined (up to one year old). Other abnormalities such as myelin outfoldings were observed in a lower proportion of cases (Fig. 8*B*III*, C*). Teased fibers from transgenic sciatic nerves also revealed presumptive tomacula, which were either symmetric (both sides of the affected node) or asymmetric (only one side affected, e.g. Fig. 8*D*). Similar asymmetry of hypermyelination was also observed (data not shown).

Rapamycin treatment prevents myelin abnormalities *in vivo*

The mTOR pathway has been previously implicated in the Akt-mediated hypermyelination in the CNS (Flores et al., 2008; Narayanan et al., 2009; Goebbels et al.,

2010) and PNS (Goebbels et al., 2012; Sherman et al., 2012; Norrmen et al., 2014). In agreement, MyrAkt activates mTOR in the PNS based on Western blot analysis of sciatic nerve lysates. Increased phosphorylation of Akt at both the S473 or Th308 residues was readily detected in the transgenics by the appearance of an extra phosphorylated Akt band resulting from the myristoylation tag (Fig. 8*E*). A statistically significant increase of phospho-S6RP (S235/236) levels, an indirect substrate of mTORC1 and readout of Akt activation, was found in samples from transgenic animals when compared to their wild type littermates (Fig. 8*E*, *F*). The levels of phospho-GSK3b (S9) and the translation repressor protein phospho-4E-BP1 (Thr37/46) were also increased in those nerves, although did not reach statistical significance. No significant differences were found for the total levels of any of these proteins (Fig. 8*F*). These results confirm that the CNP-MyrAktHA transgene is not only properly expressed, but also active in those animals.

Treatment with rapamycin for eight weeks resulted in a dramatic reduction in sciatic nerve size in MyrAkt mice (Fig. 9*A, C*) and a correction of hypermyelination (Fig. 9*A*). The efficacy of the rapamycin treatment on mTOR activity was corroborated by Western blot analysis (Fig. 9*B*). Other parameters affected in the MyrAkt transgenics, such as brain size or the number of myelin abnormalities, were also ameliorated by rapamycin treatment, and corrected to near wild type levels (Fig. 9*C*). In dorsal roots, g-ratios values were significantly increased in drug-treated versus vehicle-treated transgenics (0.59 +/- 0.02 and 0.54 +/- 0.01 respectively), although the values were still somewhat lower than their wild type littermates (0.62 +/- 0.006, Fig. 9*D*). Interestingly, no improvement of the hyperwrapping phenotype was detected in the Remak bundles of the rapamycin-treated transgenics (Fig. 9*E*). Taken together, our data indicates that mTOR activation has a key role in many but not all of the PNS phenotypes driven by activation of Akt.

DISCUSSION

PNS myelination is controlled by levels of axonal NRG1III (Michailov et al., 2004; Taveggia et al., 2005), which activates Schwann cell ErbB receptors and thereby PI3K, MAPK, and Phospholipase C-γ; each of these pathways have been implicated in myelination (Pereira et al., 2010; Pereira et al., 2012; Salzer, 2015). In the case of PI3K, pharmacological inhibition blocks myelination *in vitro* at an early stage (Maurel and Salzer, 2000) whereas PI3K gain of function, via conditional ablation of PTEN, results in hypermyelination *in vivo* with the occasional small caliber axon switching to a myelinated fate (Goebbels et al., 2010). The serine/threonine kinase Akt is a major effector of PI3K and is thus a candidate to mediate these effects in the PNS. However, a prior study of a transgenic mouse overexpressing Akt-DD in both oligodendrocytes and Schwann cells under the control of the glial promoter PLP, demonstrated hypermyelination in the CNS but not the PNS (Flores et al., 2008). This latter result raised the question of whether the effects of PI3K in the PNS are primarily mediated by Akt or result from Akt-independent signaling by PI3K (Ebi et al., 2013).

We now demonstrate that Akt is indeed a key regulator of PNS myelination based on both loss (perifosine treatment) and gain of function (transgene) analyses. The expression of a constitutively active Akt under control of the CNP promoter provides some striking similarities and interesting differences with previously reported animal models. In particular, our findings phenocopy important aspects of the PTEN conditional mice (Goebbels et al., 2010; Goebbels et al., 2012), while differing from the prior Akt transgenic mouse model (Flores et al., 2008). CNP comprises a higher percent of the total myelin protein in the PNS than does PLP (Patzig et al., 2011) indicating that the lack of a PNS effect in the previously reported PLP-AktDD transgenic mice (Flores et al., 2008) may be due to lower expression levels. In addition, we observed a more consistent hypermyelinating phenotype in the MyrAkt than in the Akt-DD

transgenics, each under the control of the CNP promoter, suggesting the membrane-targeted form of Akt is more potent in promoting hypermyelination.

The promyelinating effect of Akt shown here is consistent with evidence that axonal NRG1III is the main driver of Akt activation (Taveggia et al., 2005; Heller et al., 2014). Indeed, overexpression of NRG1III also results in hypermyelination (Michailov et al., 2004) and our results suggest Akt activation likely strongly contributes. Myelin outfolding/infoldings are also present in human mutations of MTMR13 in CMT patients and corresponding mouse models, that increase the levels of PIP4,5 (Bolis et al., 2005; Tersar et al., 2007; Robinson et al., 2008; Goebbels et al., 2012) which would not be expected to activate PI3K. Thus, other mechanisms can contribute to myelin outfoldings and tomacula in addition to hyper-activation of Akt. Interestingly, myelin outfoldings are normally present in the CNS at the peak of myelination as a consequence of active myelin production, correlated with an elevated concentration of PIP3 at the inner tongue of the process and the presence of cytoplasmic channels (Snaidero et al., 2014). These features disappear in mature CNS myelin.

Here we implicate Akt as a direct regulator of axonal sorting and wrapping, which are among the earliest events in axon-Schwann cell interactions. Thus, pharmacological reduction of Akt activity partially blocks wrapping (Fig. 2*G*) whereas MyrAkt leads to excessive wrapping in the transgenics, most evident in non-myelinating Schwann cells of Remak bundles and sympathetic fibers. A similar phenotype was also seen in PTEN conditional mice (Goebbels et al., 2010). A plausible candidate to mediate these effects is Rac1, which drives generation of radial lamellopodia in Schwann cells required for ensheathment of axons and the onset of myelination (Benninger et al., 2007; Nodari et al., 2007). PI3K activates its effectors, including Akt, by generating local concentrations of PIP3. PI3K similarly activates Rho GTPases, notably Rac, via PIP3-dependent activation of members of the Dbl family of guanine-nucleotide exchange factors (GEFs) (Innocenti et al., 2003). Results in this study (Fig. 7) indicate that Akt

490 can activate Rac1 independently of PIP3-dependent effect of PI3K on GEFs. They further
491 suggest Akt-dependent activation of Rac1 may account for the hyperwrapping and
492 hypermyelination observed in the PTEN conditional mice given the similarity of phenotypes.
493 Interestingly, the membrane outfoldings and Schwann cell pockets induced by MyrAkt
494 were not obligately coupled to axonal contact; even collagen fibers were wrapped in the
495 transgenic mice (Fig. 6*A*II). In normal nerves, Akt is activated initially along the internode, in
496 close apposition to and dependent on NRG on the axon; activated Akt is later detected at the
497 paranodes once compact myelin has formed (Heller et al., 2014). The NRG-dependent
498 activation of Akt locally, along the inner turn, thus favors specific wrapping of the apposed
499 axon. In contrast, the widespread activation of Akt along other membranes of the transgenic
500 Schwann cells, likely supports wrapping that is independent of axonal contact. Remarkably,
501 some of the Schwann cell processes lacking axonal contact were surrounded by basal lamina
502 in the transgenics (Fig. 6*A*, *B*). These results suggest that Akt may help transduce the axonal
503 signal that drives production and deposition of extracellular matrix components by Schwann
504 cells (Bunge et al., 1986).

505 A striking result of this study is that the promyelinating effects of Akt are not correlated
506 to the levels of Krox20, the key transcriptional driver of PNS myelination (Topilko et al., 1994).
507 Thus, induction of MyrAkt in Schwann cell cultures resulted in an increase, with some
508 variability, of myelin protein and mRNA levels despite a modest reduction in the basal levels of
509 Krox20 (Fig. 3). Conversely, inhibition of Schwann cell Akt by Pf partially arrests ensheathment
510 and nearly completely blocks myelin protein expression but not the upregulation of Oct6 and
511 Krox20 (Fig. 2). In the latter case, partial ensheathment of axons may have been sufficient to
512 upregulate these transcription factors whereas treatment with LY by completely abolishing
513 ensheathment, may have thereby blocked Oct6 and Krox20 expression. Together, these
514 results suggest that changes in myelin mRNA and protein levels resulting from Akt

inhibition/activation may not be transcriptionally regulated. Alternative possibilities include an effect of Akt on miRNAs or protein translation. Akt has been implicated in regulating miRNA levels via the FOXO transcription factors and MDM2/p53 activity (Xu and Mo, 2012); FOXO phosphorylation is indeed increased in the MyrAkt mice (E. Domènech-Estévez, data not shown) raising the potential of similar regulation of the Schwann cell phenotype via miRNAs (Pereira et al., 2010). In addition, Akt may control myelin protein levels by regulating their turnover and translation. A key role for translational control in myelination was shown by the rescue of myelination in ErbB deficient Schwann cells via expression of activated Mek1DD which, in turn, strikingly upregulated protein translation (Sheean et al., 2014). Like the MyrAkt transgenics, sciatic nerves in the activated Mek1 transgenic mice are hypermyelinated, with tomacular defects, and have small caliber axons that remain unmyelinated (Sheean et al., 2014). This latter result suggests that other signaling pathways downstream of NRG/ErbB activation, including the PLCγ/calcineurin/NFATc4 pathway (Kao et al., 2009), are also required for expression of the transcriptional phenotype of myelinating Schwann cells.

As in the PTEN mutants, the MyrAkt transgenics have increased mTORC1 activity, evidenced by increased phosphorylation of S6RP (Fig. 8). mTOR has a key role in Schwann cell myelination (Sherman et al., 2012). In particular, the mTORC1 complex links nutrient availability and cell growth by regulating protein and lipid synthesis (Porstmann et al., 2008; Laplante and Sabatini, 2009; Peterson et al., 2011). Mice deficient in the mTORC1 component raptor have delayed myelination and hypomyelination in the adult due to impaired RXRγ-SREBP controlled lipid biosynthesis (Norrmen et al., 2014); these results place mTORC1, and by implication Akt, as important coordinators of protein translation and lipid synthesis in the myelinating Schwann cells. Rapamycin administration dramatically reduces the pathological features of the MyrAkt transgenics, normalizing the g-ratios, number of axons per area, number of myelin abnormalities and brain weight (Fig. 9). These results corroborate the beneficial

effects of rapamycin in treating dysmyelinating pathologies resulting from deregulation of the PI3K-Akt-mTORC1 axis (Narayanan et al., 2009; Goebbels et al., 2012).

Interestingly, the hyperwrapping phenotype in the transgenics in unmyelinated Schwann cells was not blocked by rapamycin (Fig. 9*E*), presumably as hyperwrapping is driven by Rac1 and is independent of mTOR. Thus, Akt-induced wrapping and myelin production, although coordinated, are two distinct phenomena driven by independent pathways. Indeed, multiple crucial events of myelination, including morphogenesis (Benninger et al., 2007; Ozcelik et al., 2010), transcriptional activation (Zorick et al., 1996; Jacob et al., 2011), protein and lipid synthesis (Nadra et al., 2008; Norrmen et al., 2014) and metabolic status (Pooya et al., 2014) must all be tightly coordinated during Schwann cell myelination. Akt activation likely contributes to each of these events with the potential exception of Krox20-dependent transcriptional events.

In conclusion, we have shown that Akt has a key role in regulating PNS myelination, enhancing membrane wrapping potentially via Rac1 activation and myelin protein synthesis via mTORC1. These studies suggest that PI3K/Akt activation has a key role and cooperates with other signaling pathways during the shift from the ensheathing to the myelinating Schwann cell phenotype. Our data additionally suggest that myelin abnormalities in various neuropathies, including in/outfoldings and tomacula, may result from Akt activation and highlight Akt and its effectors, as potential therapeutic targets. Akt activation would be expected to ameliorate the phenotype of hypomyelinating peripheral neuropathies, e.g. CMT4C (Arnaud et al., 2009; Gouttenoire et al., 2013) whereas Akt inhibition would be a candidate to ameliorate tomacular defects in neuropathies such as HNPP (Sander et al., 2000; Goebbels et al., 2012). Further studies of Akt-dependent pathways in myelination may identify more specific therapeutic targets for these neuropathies in the future.

REFERENCES

Adlkofer K, Frei R, Neuberg DH, Zielasek J, Toyka KV, Suter U (1997) Heterozygous peripheral myelin protein 22-deficient mice are affected by a progressive demyelinating tomaculous neuropathy. J Neurosci 17:4662-4671.

Arnaud E, Zenker J, de Preux Charles AS, Stendel C, Roos A, Medard JJ, Tricaud N, Kleine H, Luscher B, Weis J, Suter U, Senderek J, Chrast R (2009) SH3TC2/KIAA1985 protein is required for proper myelination and the integrity of the node of Ranvier in the peripheral nervous system. Proceedings of the National Academy of Sciences of the United States of America 106:17528-17533.

Benninger Y, Thurnherr T, Pereira JA, Krause S, Wu X, Chrostek-Grashoff A, Herzog D, Nave KA, Franklin RJ, Meijer D, Brakebusch C, Suter U, Relvas JB (2007) Essential and distinct roles for cdc42 and rac1 in the regulation of Schwann cell biology during peripheral nervous system development. J Cell Biol 177:1051-1061.

Bolino A, Bolis A, Previtali SC, Dina G, Bussini S, Dati G, Amadio S, Del Carro U, Mruk DD, Feltri ML, Cheng CY, Quattrini A, Wrabetz L (2004) Disruption of Mtmr2 produces CMT4B1-like neuropathy with myelin outfolding and impaired spermatogenesis. J Cell Biol 167:711-721.

Bolis A, Coviello S, Bussini S, Dina G, Pardini C, Previtali SC, Malaguti M, Morana P, Del Carro U, Feltri ML, Quattrini A, Wrabetz L, Bolino A (2005) Loss of Mtmr2 phosphatase in Schwann cells but not in motor neurons causes Charcot-Marie-Tooth type 4B1 neuropathy with myelin outfoldings. J Neurosci 25:8567-8577.

Bunge RP, Bunge MB, Eldridge CF (1986) Linkage between axonal ensheathment and basal lamina production by Schwann cells. Annual review of neuroscience 9:305-328.

588 Chandross KJ, Cohen RI, Paras P, Jr., Gravel M, Braun PE, Hudson LD (1999) Identification
589 and characterization of early glial progenitors using a transgenic selection strategy. J
590 Neurosci 19:759-774.
591 Cho H, Thorvaldsen JL, Chu Q, Feng F, Birnbaum MJ (2001a) Akt1/PKBalpha is required for
592 normal growth but dispensable for maintenance of glucose homeostasis in mice. J Biol
593 Chem 276:38349-38352.
594 Cho H, Mu J, Kim JK, Thorvaldsen JL, Chu Q, Crenshaw EB, 3rd, Kaestner KH, Bartolomei
595 MS, Shulman GI, Birnbaum MJ (2001b) Insulin resistance and a diabetes mellitus-like
596 syndrome in mice lacking the protein kinase Akt2 (PKB beta). Science 292:1728-1731.
597 Cotter L, Ozcelik M, Jacob C, Pereira JA, Locher V, Baumann R, Relvas JB, Suter U, Tricaud
598 N (2010) Dlg1-PTEN interaction regulates myelin thickness to prevent damaging
599 peripheral nerve overmyelination. Science 328:1415-1418.
600 Decker L, Desmarquet-Trin-Dinh C, Taillebourg E, Ghislain J, Vallat JM, Charnay P (2006)
601 Peripheral myelin maintenance is a dynamic process requiring constant Krox20
602 expression. J Neurosci 26:9771-9779.
603 Deinhardt K, Kim T, Spellman DS, Mains RE, Eipper BA, Neubert TA, Chao MV, Hempstead
604 BL (2011) Neuronal growth cone retraction relies on proneurotrophin receptor signaling
605 through Rac. Science signaling 4:ra82.
606 Easton RM, Cho H, Roovers K, Shineman DW, Mizrahi M, Forman MS, Lee VM, Szabolcs M,
607 de Jong R, Oltersdorf T, Ludwig T, Efstratiadis A, Birnbaum MJ (2005) Role for
608 Akt3/protein kinase Bgamma in attainment of normal brain size. Mol Cell Biol 25:1869-
609 1878.
610 Ebi H, Costa C, Faber AC, Nishtala M, Kotani H, Juric D, Della Pelle P, Song Y, Yano S, Mino-
611 Kenudson M, Benes CH, Engelman JA (2013) PI3K regulates MEK/ERK signaling in

612 breast cancer via the Rac-GEF, P-Rex1. Proceedings of the National Academy of
613 Sciences of the United States of America 110:21124-21129.
614 Flores AI, Narayanan SP, Morse EN, Shick HE, Yin X, Kidd G, Avila RL, Kirschner DA, Macklin
615 WB (2008) Constitutively active Akt induces enhanced myelination in the CNS. J
616 Neurosci 28:7174-7183.
617 Franke TF (2008) PI3K/Akt: getting it right matters. Oncogene 27:6473-6488.
618 Franke TF, Yang SI, Chan TO, Datta K, Kazlauskas A, Morrison DK, Kaplan DR, Tsichlis PN
619 (1995) The protein kinase encoded by the Akt proto-oncogene is a target of the PDGF-
620 activated phosphatidylinositol 3-kinase. Cell 81:727-736.
621 Gills JJ, Dennis PA (2009) Perifosine: update on a novel Akt inhibitor. Curr Oncol Rep 11:102-
622 110.
623 Goebbels S, Oltrogge JH, Wolfer S, Wieser GL, Nientiedt T, Pieper A, Ruhwedel T, Groszer M,
624 Sereda MW, Nave KA (2012) Genetic disruption of Pten in a novel mouse model of
625 tomaculous neuropathy. EMBO molecular medicine 4:486-499.
626 Goebbels S, Oltrogge JH, Kemper R, Heilmann I, Bormuth I, Wolfer S, Wichert SP, Mobius W,
627 Liu X, Lappe-Siefke C, Rossner MJ, Groszer M, Suter U, Frahm J, Boretius S, Nave KA
628 (2010) Elevated phosphatidylinositol 3,4,5-trisphosphate in glia triggers cell-
629 autonomous membrane wrapping and myelination. J Neurosci 30:8953-8964.
630 Gouttenoire EA, Lupo V, Calpena E, Bartesaghi L, Schupfer F, Medard JJ, Maurer F,
631 Beckmann JS, Senderek J, Palau F, Espinos C, Chrast R (2013) Sh3tc2 deficiency
632 affects neuregulin-1/ErbB signaling. Glia 61:1041-1051.
633 Gravel M, Di Polo A, Valera PB, Braun PE (1998) Four-kilobase sequence of the mouse CNP
634 gene directs spatial and temporal expression of lacZ in transgenic mice. Journal of
635 neuroscience research 53:393-404.

636 Heller BA, Ghidinelli M, Voelkl J, Einheber S, Smith R, Grund E, Morahan G, Chandler D,
637 Kalaydjieva L, Giancotti F, King RH, Fejes-Toth AN, Fejes-Toth G, Feltri ML, Lang F,
638 Salzer JL (2014) Functionally distinct PI 3-kinase pathways regulate myelination in the
639 peripheral nervous system. J Cell Biol 204:1219-1236.
640 Hennessy BT, Lu Y, Poradosu E, Yu Q, Yu S, Hall H, Carey MS, Ravoori M, Gonzalez-Angulo
641 AM, Birch R, Henderson IC, Kundra V, Mills GB (2007) Pharmacodynamic markers of
642 perifosine efficacy. Clin Cancer Res 13:7421-7431.
643 Innocenti M, Frittoli E, Ponzanelli I, Falck JR, Brachmann SM, Di Fiore PP, Scita G (2003)
644 Phosphoinositide 3-kinase activates Rac by entering in a complex with Eps8, Abi1, and
645 Sos-1. J Cell Biol 160:17-23.
646 Jacob C, Christen CN, Pereira JA, Somandin C, Baggiolini A, Lotscher P, Ozcelik M, Tricaud
647 N, Meijer D, Yamaguchi T, Matthias P, Suter U (2011) HDAC1 and HDAC2 control the
648 transcriptional program of myelination and the survival of Schwann cells. Nature
649 neuroscience 14:429-436.
650 Kao SC, Wu H, Xie J, Chang CP, Ranish JA, Graef IA, Crabtree GR (2009) Calcineurin/NFAT
651 signaling is required for neuregulin-regulated Schwann cell differentiation. Science
652 323:651-654.
653 Kidd GJ, Ohno N, Trapp BD (2013) Biology of Schwann cells. Handbook of clinical neurology
654 115:55-79.
655 Laplante M, Sabatini DM (2009) mTOR signaling at a glance. Journal of cell science 122:3589-
656 3594.
657 Leavens KF, Easton RM, Shulman GI, Previs SF, Birnbaum MJ (2009) Akt2 is required for
658 hepatic lipid accumulation in models of insulin resistance. Cell Metab 10:405-418.

659 Matsui T, Li L, del Monte F, Fukui Y, Franke TF, Hajjar RJ, Rosenzweig A (1999) Adenoviral
660 gene transfer of activated phosphatidylinositol 3'-kinase and Akt inhibits apoptosis of
661 hypoxic cardiomyocytes in vitro. Circulation 100:2373-2379.
662 Maurel P, Salzer JL (2000) Axonal regulation of Schwann cell proliferation and survival and the
663 initial events of myelination requires PI 3-kinase activity. J Neurosci 20:4635-4645.
664 Michailov GV, Sereda MW, Brinkmann BG, Fischer TM, Haug B, Birchmeier C, Role L, Lai C,
665 Schwab MH, Nave KA (2004) Axonal neuregulin-1 regulates myelin sheath thickness.
666 Science 304:700-703.
667 Mirsky R, Woodhoo A, Parkinson DB, Arthur-Farraj P, Bhaskaran A, Jessen KR (2008) Novel
668 signals controlling embryonic Schwann cell development, myelination and
669 dedifferentiation. Journal of the peripheral nervous system : JPNS 13:122-135.
670 Monk KR, Feltri ML, Taveggia C (2015) New insights on schwann cell development. Glia.
671 Nadra K, de Preux Charles AS, Medard JJ, Hendriks WT, Han GS, Gres S, Carman GM,
672 Saulnier-Blache JS, Verheijen MH, Chrast R (2008) Phosphatidic acid mediates
673 demyelination in Lpin1 mutant mice. Genes & development 22:1647-1661.
674 Narayanan SP, Flores AI, Wang F, Macklin WB (2009) Akt signals through the mammalian
675 target of rapamycin pathway to regulate CNS myelination. J Neurosci 29:6860-6870.
676 Nave KA, Salzer JL (2006) Axonal regulation of myelination by neuregulin 1. Current opinion in
677 neurobiology 16:492-500.
678 Nave KA, Werner HB (2014) Myelination of the nervous system: mechanisms and functions.
679 Annual review of cell and developmental biology 30:503-533.
680 Newbern J, Birchmeier C (2010) Nrg1/ErbB signaling networks in Schwann cell development
681 and myelination. Seminars in cell & developmental biology 21:922-928.

682 Nodari A, Zambroni D, Quattrini A, Court FA, D'Urso A, Recchia A, Tybulewicz VL, Wrabetz L,
683 Feltri ML (2007) Beta1 integrin activates Rac1 in Schwann cells to generate radial
684 lamellae during axonal sorting and myelination. J Cell Biol 177:1063-1075.
685 Norrmen C, Figlia G, Lebrun-Julien F, Pereira JA, Trotzmuller M, Kofeler HC, Rantanen V,
686 Wessig C, van Deijk AL, Smit AB, Verheijen MH, Ruegg MA, Hall MN, Suter U (2014)
687 mTORC1 controls PNS myelination along the mTORC1-RXRgamma-SREBP-lipid
688 biosynthesis axis in Schwann cells. Cell reports 9:646-660.
689 Noseda R, Belin S, Piguet F, Vaccari I, Scarlino S, Brambilla P, Martinelli Boneschi F, Feltri
690 ML, Wrabetz L, Quattrini A, Feinstein E, Huganir RL, Bolino A (2013)
691 DDIT4/REDD1/RTP801 is a novel negative regulator of Schwann cell myelination. J
692 Neurosci 33:15295-15305.
693 Ogata T, Iijima S, Hoshikawa S, Miura T, Yamamoto S, Oda H, Nakamura K, Tanaka S (2004)
694 Opposing extracellular signal-regulated kinase and Akt pathways control Schwann cell
695 myelination. J Neurosci 24:6724-6732.
696 Ozcelik M, Cotter L, Jacob C, Pereira JA, Relvas JB, Suter U, Tricaud N (2010) Pals1 is a
697 major regulator of the epithelial-like polarization and the extension of the myelin sheath
698 in peripheral nerves. J Neurosci 30:4120-4131.
699 Patzig J, Jahn O, Tenzer S, Wichert SP, de Monasterio-Schrader P, Rosfa S, Kuharev J, Yan
700 K, Bormuth I, Bremer J, Aguzzi A, Orfaniotou F, Hesse D, Schwab MH, Mobius W,
701 Nave KA, Werner HB (2011) Quantitative and integrative proteome analysis of
702 peripheral nerve myelin identifies novel myelin proteins and candidate neuropathy loci.
703 J Neurosci 31:16369-16386.
704 Pereira JA, Lebrun-Julien F, Suter U (2012) Molecular mechanisms regulating myelination in
705 the peripheral nervous system. Trends in neurosciences 35:123-134.

706 Pereira JA, Baumann R, Norrmen C, Somandin C, Miehe M, Jacob C, Luhmann T, Hall-Bozic
707 H, Mantei N, Meijer D, Suter U (2010) Dicer in Schwann cells is required for myelination
708 and axonal integrity. J Neurosci 30:6763-6775.
709 Peterson TR, Sengupta SS, Harris TE, Carmack AE, Kang SA, Balderas E, Guertin DA,
710 Madden KL, Carpenter AE, Finck BN, Sabatini DM (2011) mTOR complex 1 regulates
711 lipin 1 localization to control the SREBP pathway. Cell 146:408-420.
712 Pooya S, Liu X, Kumar VB, Anderson J, Imai F, Zhang W, Ciraolo G, Ratner N, Setchell KD,
713 Yutaka Y, Jankowski MP, Dasgupta B (2014) The tumour suppressor LKB1 regulates
714 myelination through mitochondrial metabolism. Nature communications 5:4993.
715 Porstmann T, Santos CR, Griffiths B, Cully M, Wu M, Leevers S, Griffiths JR, Chung YL,
716 Schulze A (2008) SREBP activity is regulated by mTORC1 and contributes to Akt-
717 dependent cell growth. Cell Metab 8:224-236.
718 Robinson FL, Niesman IR, Beiswenger KK, Dixon JE (2008) Loss of the inactive myotubularin-
719 related phosphatase Mtmr13 leads to a Charcot-Marie-Tooth 4B2-like peripheral
720 neuropathy in mice. Proceedings of the National Academy of Sciences of the United
721 States of America 105:4916-4921.
722 Salzer JL (2015) Schwann cell myelination. Cold Spring Harbor perspectives in biology
723 7:a020529.
724 Sander S, Ouvrier RA, McLeod JG, Nicholson GA, Pollard JD (2000) Clinical syndromes
725 associated with tomacula or myelin swellings in sural nerve biopsies. Journal of
726 neurology, neurosurgery, and psychiatry 68:483-488.
727 Sheean ME, McShane E, Cheret C, Walcher J, Muller T, Wulf-Goldenberg A, Hoelper S,
728 Garratt AN, Kruger M, Rajewsky K, Meijer D, Birchmeier W, Lewin GR, Selbach M,
729 Birchmeier C (2014) Activation of MAPK overrides the termination of myelin growth and

730 replaces Nrg1/ErbB3 signals during Schwann cell development and myelination. Genes
731 & development 28:290-303.
732 Sherman DL, Krols M, Wu LM, Grove M, Nave KA, Gangloff YG, Brophy PJ (2012) Arrest of
733 myelination and reduced axon growth when Schwann cells lack mTOR. J Neurosci
734 32:1817-1825.
735 Snaidero N, Mobius W, Czopka T, Hekking LH, Mathisen C, Verkleij D, Goebbels S, Edgar J,
736 Merkler D, Lyons DA, Nave KA, Simons M (2014) Myelin membrane wrapping of CNS
737 axons by PI(3,4,5)P3-dependent polarized growth at the inner tongue. Cell 156:277-
738 290.
739 Taveggia C, Zanazzi G, Petrylak A, Yano H, Rosenbluth J, Einheber S, Xu X, Esper RM, Loeb
740 JA, Shrager P, Chao MV, Falls DL, Role L, Salzer JL (2005) Neuregulin-1 type III
741 determines the ensheathment fate of axons. Neuron 47:681-694.
742 Tersar K, Boentert M, Berger P, Bonneick S, Wessig C, Toyka KV, Young P, Suter U (2007)
743 Mtmr13/Sbf2-deficient mice: an animal model for CMT4B2. Hum Mol Genet 16:2991-
744 3001.
745 Thurnherr T, Benninger Y, Wu X, Chrostek A, Krause SM, Nave KA, Franklin RJ, Brakebusch
746 C, Suter U, Relvas JB (2006) Cdc42 and Rac1 signaling are both required for and act
747 synergistically in the correct formation of myelin sheaths in the CNS. J Neurosci
748 26:10110-10119.
749 Topilko P, Schneider-Maunoury S, Levi G, Baron-Van Evercooren A, Chennoufi AB, Seitanidou
750 T, Babinet C, Charnay P (1994) Krox-20 controls myelination in the peripheral nervous
751 system. Nature 371:796-799.
752 Tschopp O, Yang ZZ, Brodbeck D, Dummler BA, Hemmings-Mieszczak M, Watanabe T,
753 Michaelis T, Frahm J, Hemmings BA (2005) Essential role of protein kinase B gamma

(PKB gamma/Akt3) in postnatal brain development but not in glucose homeostasis. Development 132:2943-2954.

Vlahos CJ, Matter WF, Hui KY, Brown RF (1994) A specific inhibitor of phosphatidylinositol 3-kinase, 2-(4-morpholinyl)-8-phenyl-4H-1-benzopyran-4-one (LY294002). J Biol Chem 269:5241-5248.

Xu M, Mo YY (2012) The Akt-associated microRNAs. Cellular and molecular life sciences : CMLS 69:3601-3612.

Zanazzi G, Einheber S, Westreich R, Hannocks MJ, Bedell-Hogan D, Marchionni MA, Salzer JL (2001) Glial growth factor/neuregulin inhibits Schwann cell myelination and induces demyelination. J Cell Biol 152:1289-1299.

Zorick TS, Syroid DE, Arroyo E, Scherer SS, Lemke G (1996) The Transcription Factors SCIP and Krox-20 Mark Distinct Stages and Cell Fates in Schwann Cell Differentiation. Mol Cell Neurosci 8:129-145.

FIGURE LEGENDS

Figure 1. Loss of individual Akt isoforms *in vivo* does not affect PNS myelination.

A, Western blot analysis of the expression of the three Akt isoforms in dorsal root ganglia neurons (Neu), Schwann cells (SC), and non-myelinated (C) or myelinated (C+C) cocultures. Akt1 and Akt3 are preferentially expressed by neurons whereas Akt2 is primarily expressed by Schwann cells. n=3. SEM is shown. ***B*****,** Semithin sections of sciatic nerves from two month-old mice deficient in each Akt isoform revealed no obvious defects of myelination. Left panels show a magnification of the inset from the semithin section. Right panels (a-f) show representative images of Remak bundles. No abnormalities of myelination or ensheathment were evident at the time point analyzed, although no quantifications were performed. Scale bars for semithin 100 µm, for EM 2 µm.

Figure 2. Akt inhibition blocks myelin formation *in vitro* without affecting Krox20 levels.

A, Treatment of DRG neuron-Schwann cell cocultures with perifosine (Pf) or LY294002 (LY) blocked myelination. The myelin transcription factors Krox20 and Oct6 continue to be robustly expressed by Schwann cells in the Pf but not the LY treated cocultures. n=5, four coverslips were analyzed for each n. ***B*****,** Quantification of the blockade of myelination by Pf and LY. The average number of myelin segments per coverslip were: controls, 2195; Pf, 37 (p=0.0056); and LY, 3 segments (p=0.005). n=3, each n represents two coverslips. ***C***,***D*****,** Pf treated cells showed no change in Krox20 protein expression (102.8 +/- 12.31, p=0.83), although a significant decrease in pAkt 473 (40.1 +/- 7.77, p=0.001), MBP (3.1 +/- 0.2, p<0.001) and P0 (12.5 +/- 4.49, p<0.001) was detected. The same markers were also downregulated in LY treated cocultures (pAkt 26.7 +/- 6.84, p<0.001; MBP 1.6 +/- 1.03, p<0.001; P0 1.69 +/- 0.68, p<0.001), but in this case Krox20 was also decreased (22.1 +/- 5.86, p<0.001) (n=3, each n represents eight coverslips pooled per condition). Western blot quantification data were normalized using

values from control cocultures that were arbitrarily set to 100. ***E*****,** As detected by real time PCR, Pf treated cells showed no changes in Krox20 mRNA (1.27 +/- 0.39, p=0.51), and a significant decrease of mRNA for MBP (0.13 +/- 0.03, p<0.001). A decrease of P0 was also detected, although it did not reach statistical significance (0.62 +/- 0.18 p=0.09). These three markers where significantly downregulated in LY treated cocultures (Krox20 0.12 +/- 0.04, p<0.001; MBP 0.01 +/- 0.003, p<0.001; P0 0.23 +/- 0.06, p<0.001). Expression data was normalized to control samples that were arbitrarily set as 1; GAPDH expression was used as reference. n=4, four coverslips were pooled per condition for each n. ***F***, Schwann cell proliferation was not affected by 20 μM of Pf (11.9 +/- 0.019 vs Control 11.2 +/- 0.02), whereas proliferation was almost absent with 20 μM of LY treatment (0.7 +/- 0.002, p=0.003). n=4, each n represents three coverslips per condition. ***G***, EM analysis of control, Pf and LY treated cultures revealed drug-specific differences. In the presence of Pf, Schwann cells (SC) engaged axons (A) and partially but incompletely sorted them and failed to myelinate. LY treated Schwann cells completely failed to sort axons. The image depicts representative fields from the cultures shown in ***A***. Scale bars: 1 μm. SEM is shown in all panels.

Figure 3. Akt activation promotes myelin formation independently of Krox20 regulation. Purified Schwann cells infected with doxycycline (Dox) inducible lentiviruses encoding MyrAkt-HA or GFP were cultured in ascorbic acid containing media in the absence of axons. ***A***, GFP induction with Dox did not affect the basal levels of protein for Krox20, P0 and MAG. Basal levels for MAG were not detectable for quantification. n=3. ***B***, ***C*** Induction of MyrAkt substantially increased P0 protein levels (358.1, 586.7 and 1114.5 folds vs 100, average 686.5 +/- 223.98, p=0.058) and significantly increased MAG levels (3541.7, 9467.8 and 6717.2 folds vs 100, average 6575.6 +/- 1712.19, p=0.045), as detected by Western blot. Interestingly, a modest but significant reduction of Krox20 was also detected (83.8 +/- 5.28, p=0.037). Western

820 blot quantification data were normalizing by using values from control samples that were
821 arbitrarily set to 100. n=3. SEM is shown. ***D***, Krox20 mRNA expression remained unchanged
822 (0.77 +/- 0.19, *p*=0.27) when Akt was induced with doxycycline. mRNA for P0 and MAG were
823 increased when Akt was induced, although due to the variability of induction (P0 1.7, 3.5 and
824 1.9 folds versus 1, average 2.4 +/- 0.57, *p*=0.07, and MAG 17.9, 168.9 and 42.2 folds versus 1,
825 average 76.3 +/- 46.81, *p*=0.18) compared to the non-induced, the increase in these markers
826 did not achieve significance by the T-test. Real time PCR data were normalized by using
827 values from control samples that were arbitrarily set to 1. GAPDH was used as a reference.
828 n=3. SEM is shown.
829
830 **Figure 4. Constitutively active Akt promotes CNS and PNS hypermyelination.**
831 ***A***, Scheme illustrating the two constitutively active Akt1 constructs driven by the CNP promoter
832 that were used to establish transgenic mice. ***B***, The HA-tagged construct was weakly
833 detectable in E13.5 dorsal root ganglia isolated from transgenic mice and readily detectable in
834 sciatic nerves (SN) from P0.5 until adulthood, with a peak at P10 that correlates with active
835 myelination. ***C***, One-year-old transgenic mice carrying the MyrAkt transgene developed
836 enlarged neural structures. Optic nerves (asterisk indicates the optic chiasm), brains, and
837 sciatic nerves were all enlarged. ***D***, HA was detectable in satellite cells from 2 month-old
838 mouse dorsal root ganglia without any obvious presence in neurons. In 2 month-old sciatic
839 nerves, HA was present with variable intensity in Schwann cells. Scale bars 20 μm. ***E***, Four
840 month-old transgenic brains (MyrAkt) were bigger than wild types (WT), with a thicker corpus
841 callosum (delineated in blue) and increased MBP staining, evidence of enhanced myelination.
842 Scale bar 1 mm.
843
844 **Figure 5. Nerves from transgenic mice are hypermyelinated.**

A, At five months, sciatic and optic nerves from MyrAkt transgenics were enlarged compared to wild types (WT) mice, as seen in transverse, toluidine blue stained sections (scale bar 100 μm). ***B***, EM sections show thicker myelin sheaths in 5 month-old MyrAkt and AktDD sciatic nerves. Optic nerves from MyrAkt were also hypermyelinated. Scale bar: sciatic nerve 10 μm, optic nerve 2 μm. ***C***, The myelin sheaths in transgenic nerves had increased numbers of myelin lamellae, scale bar 1 μm; higher magnification revealed no change in the periodicity of the myelin lamellae, scale bar 100 nm. ***D***, g-ratio analysis revealed hypermyelination was more pronounced in small caliber axons (0.5 to 2 microns). ***E***, Average g-ratio in the transgenic dorsal root was lower than in wild types (0.62 +/- 0.01 vs 0.67 +/- 0.01 respectively, p=0.02). 250 - 300 axons between 0.5 to 8 microns were measured. This difference was accentuated when only small caliber axons (0.5 to 2 microns) were considered (0.52 +/- 0.004 vs 0.61 +/- 0.01, p=0.002). n=3. SEM shown. ***F***, The numbers of Schwann cell nuclei were comparable in WT and MyrAkt dorsal roots (216 +/- 9.7 vs 250 +/- 29.2, respectively) and ventral roots (82 +/- 5.5 vs. 94 +/- 8.1, respectively) from 5 months old animals. n = 4. SEM is shown.

Figure 6. Activated Akt enhances wrapping and sorting but not myelination of axons in Remak Schwann cells.

A, EM micrographs from 20 month-old mice reveal aberrant axon-Schwann cell relationships in Remak bundles in transgenic compared to WT mice. Small axons were often surrounded by circumferential layers of uncompacted Schwann cell membranes (I, shown at higher magnification in insert). Schwann cell membranes surrounding collagen fibers (II) were also present in the transgenic nerves and were frequently covered by basal lamina. Scale bar 1 μm ***B***, In 5 month old-mice, Schwann cell processes (I), with associated basal lamina without apparent axonal contact are present; arrowheads demarcate basal lamina deposition. Schwann cells also formed empty pockets with basal lamina deposited in the interior (II arrow in the

insert); scale bars 2 μm. ***C***, Bar graph showing the distribution of the numbers of axons per Schwann cell; Remak bundles with only a few axons (1-5) are increased in the 5 month-old transgenic mice. ***D***, The number of axons per pocket was also decreased in the 5 month-old Tg suggesting better segregation of axons (one axon per pocket WT 89.12 +/- 0.007 vs Tg 96.12 +/- 1.17, *p*=0.027; two to ten axons WT 10.59 +/- 0.28 vs Tg 3.83 +/- 1.22, *p*=0.03; eleven to twenty axons WT 0.28 +/- 0.28 vs Tg 0.04 +/- 0.04, not significant). n=2, 100 bundles from sciatic nerves were analyzed per animal. ***E***, Electron micrographs of the sympathetic tract from 20 month-old mice are shown. No myelinated fibers are present but multilammelar wrapping of axons and collagen fibrils are seen consistent with a role of Akt in wrapping. Scale bar 500 nm. ***F***, The numbers of myelinated axons in transgenic dorsal (DR) and ventral (VR) roots at 5 months were not statistically different in MyrAkt vs WT mice; n=2. SEM is shown in panels *D* and *F*.

Figure 7. **MyrAkt induces Rac1 activity in cultured Schwann cells.**

A, Western blot showing the controls (GDP, GTPγS and GST) as well as samples from non-induced (-DOX) and doxycycline-induced (+DOX) Schwann cell pools transfected with the MyrAkt construct. The same –DOX and +DOX samples were loaded into two consecutive lines. ***B***, Quantification of Rac1 and cdc42 levels. Values shown represent active GTPase levels divided by total GTPase levels and corrected for actin, which served as a loading control. All data were normalized to non-induced controls, which were set to 100. Induction of MyrAkt by addition of doxycycline to the culture media increased Rac1 activity significantly (193 +/- 25.31, *p*=0.01) but not cdc42 (96.82 +/- 27.11, *p*=0.91). After correction for total cdc42 and loading amounts, the level of active cdc42 in panel A is not significantly increased. SEM is shown. Rac1: n=4 independent sets of experiments, cdc42: n=3 independent sets of experiments.

Figure 8. Sciatic nerves of MyrAkt transgenic mice exhibit tomacular defects and activation of mTOR.

A, Upper panels: Longitudinal electron micrographs of sciatic nerves from five month-old WT animals. Nodes are indicated by asterisk and the clefts by arrows. Lower panels: Longitudinal electron micrographs of sciatic nerves from transgenic animals reveal myelin infolding at the paranodes (left panel) and tomacula near the clefts (indicated with arrows) resulting in compression of the axon (right panel). Scale bars 5 μm. ***B***, Example of the different myelin abnormalities observed in sciatic nerves: I, tomacula, showing compression of the axon; II, infolding and III, outfolding. Scale bars 5 μm. ***C***, Percentages for each of the major myelin abnormalities found in cross-sections from 3 months-old transgenic sciatic nerves. n=3. ***D***, Teased fibers from six-month-old transgenic mice show an example of an asymmetric tomacular defect with enlargement in the paranodal region of the left myelin sheath but not the right myelin sheath (asterisk marks node). ***E***, Western blot analysis of extracts from nerves from 2 month-old WT and transgenic mice show activation of the mTOR pathway. ***F***, Quantification of Western blots demonstrates phosphorylated S6RP is increased in Tg nerves (218.4 +/- 25.79, p=0.01) and the ratio of phosphorylated to total S6RP is also increased (167.1 +/- 16.04, p=0.014); data were normalized to WT values arbitrarily set to 100. Increased phosphorylation of GSK3b and 4EBP1 were also evident but did not reach statistical significance. n=3. SEM is shown.

Figure 9. Rapamycin treatment reduces myelin abormalities in CNP-MyrAkt transgenic mice.

A, The phenotype of three month-old transgenic mice was largely corrected by treatment with rapamycin for eight weeks (MyrAkt+Rapa) but not by vehicle (MyrAkt+vehi); no changes were detected in control animals treated with vehicle (WT+Vehi). ***B***, Phosphorylation of S6RP was

substantially decreased in the nerves of WT and MyrAkt mice treated with rapamycin. ***C***, Analysis of several parameters are shown for WT mice treated with vehicle, and for transgenics (Myr) treated either with vehicle or rapamycin. These include brain weight (WT+Vehi 393 mg +/- 6.3; Myr+Vehi 438 +/- 10.2, *p*=0.019; Myr+Rapa 371+/- 4.75, *p*=0.004), the number of axons per 100 μm^2 (WT+Vehi 3.4 +/- 0.2; Myr+Vehi 2.3 +/- 0.07, *p*=0.01; Myr+Rapa 3.6 +/- 0.18, *p*=0.002) and the ratio of myelin abnormalities (i.e. tomacula and myelin in/outfoldings)/total axons counted (WT+Vehi 0.2% defect +/- 0.03; Myr+Vehi 3.6% +/- 0.6, *p*=0.003; Myr+Rapa 0.67% +/- 0.14, *p*=0.006). n=3. More than 3000 axons per n were examined to obtain the percentage of abnormalities. SEM is shown. ***D***, G-ratios were measured for small myelinated fibers in the dorsal roots of wild type mice on vehicle (WT+V), transgenics on Vehicle (Myr+V) and transgenics treated with rapamycin (Myr+R). Quantification of WT+Vehi (0.62 +/- 0.006), Myr+Vehi (0.54 +/- 0.01, *p*<0.001) and Myr+Rapa (0.59 +/- 0.02, *p*=0.048) demonstrates a significant increase in the g-ratio of transgenic mice treated with rapamycin. 112 - 175 small caliber axons (0.5 to 2 µm) were measured per condition. n=4. SEM is shown. ***E***, Rapamycin administration does not prevent the excess of membrane wrapping in the Remak bundles from 3 months old MyrAkt nerves. Schwann cells are pseudocolored in yellow and axons in the bundle in blue. Scale bar 1 µm.

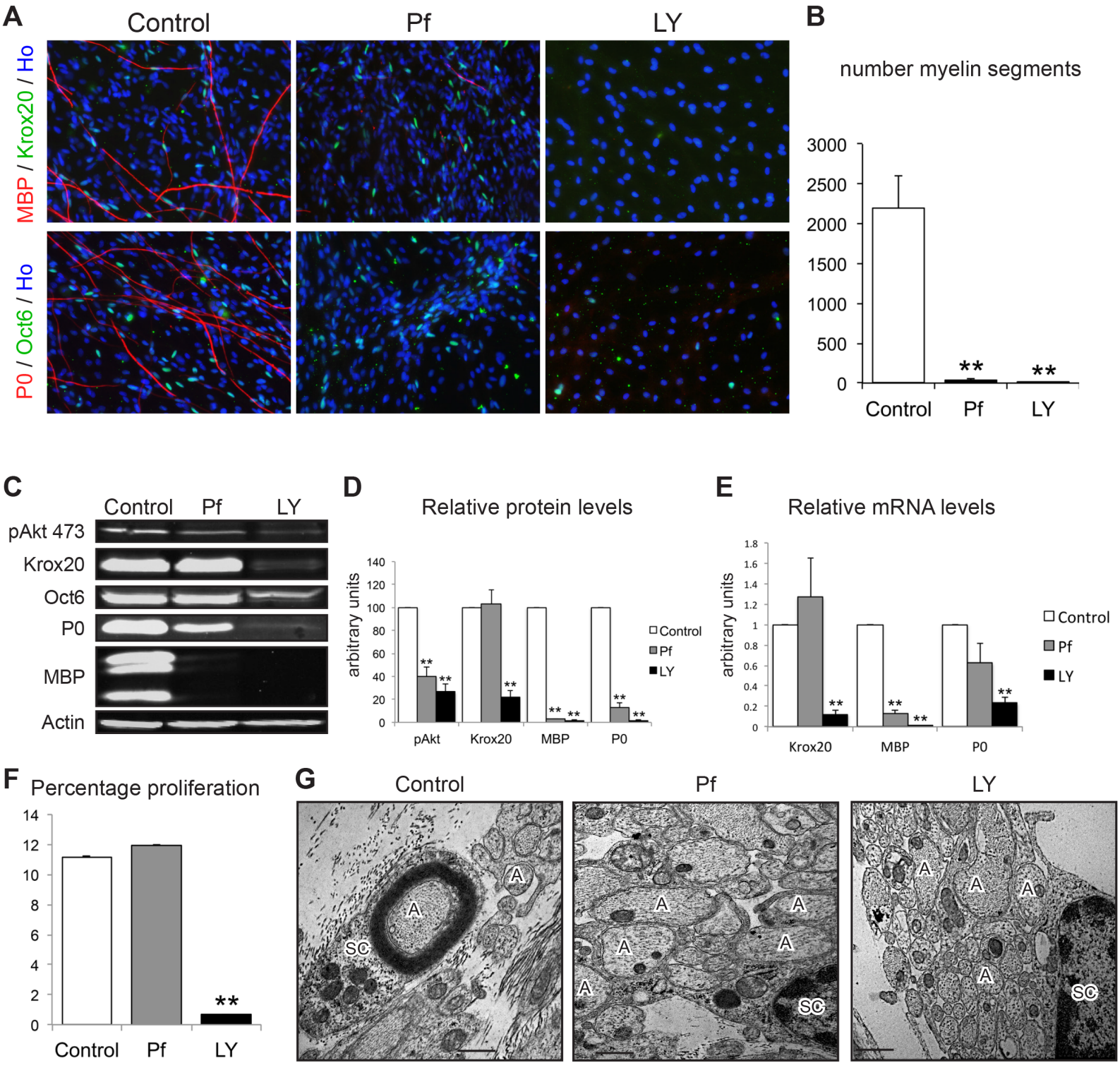
A
Control
Pf
LY
MBP / Krox20 / Ho
P0 / Oct6 / Ho
B
number myelin segments
3000
2500
2000
1500
1000
500
0
**
**
Control
Pf
LY
C
Control
Pf
LY
pAkt 473
Krox20
Oct6
P0
MBP
Actin
D
Relative protein levels
arbitrary units
140
120
100
80
60
40
20
0
**
pAkt
Krox20
MBP
P0
Control
Pf
LY
E
Relative mRNA levels
arbitrary units
1.8
1.6
1.4
1.2
1
0.8
0.6
0.4
0.2
0
Krox20
MBP
P0
Control
Pf
LY
F
Percentage proliferation
14
12
10
8
6
4
2
0
**
Control
Pf
LY
G
Control
Pf
LY
A
SC

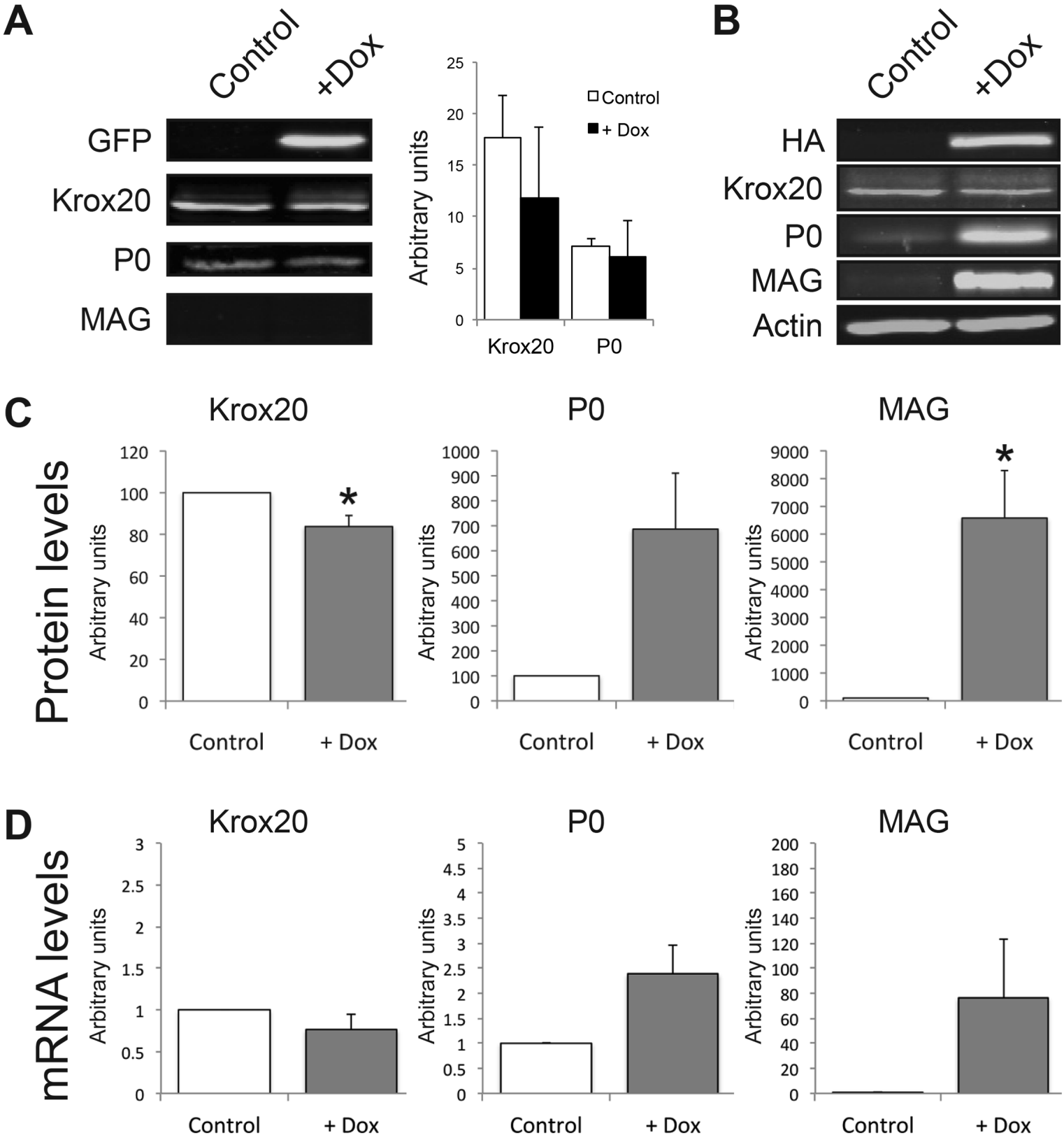
A
Control
+Dox
GFP
Krox20
P0
MAG
Arbitrary units
Control
+ Dox
Krox20
P0
B
Control
+Dox
HA
Krox20
P0
MAG
Actin
C
Protein levels
Krox20
P0
MAG
Arbitrary units
Control
+ Dox
*
D
mRNA levels
Krox20
P0
MAG
Arbitrary units
Control
+ Dox

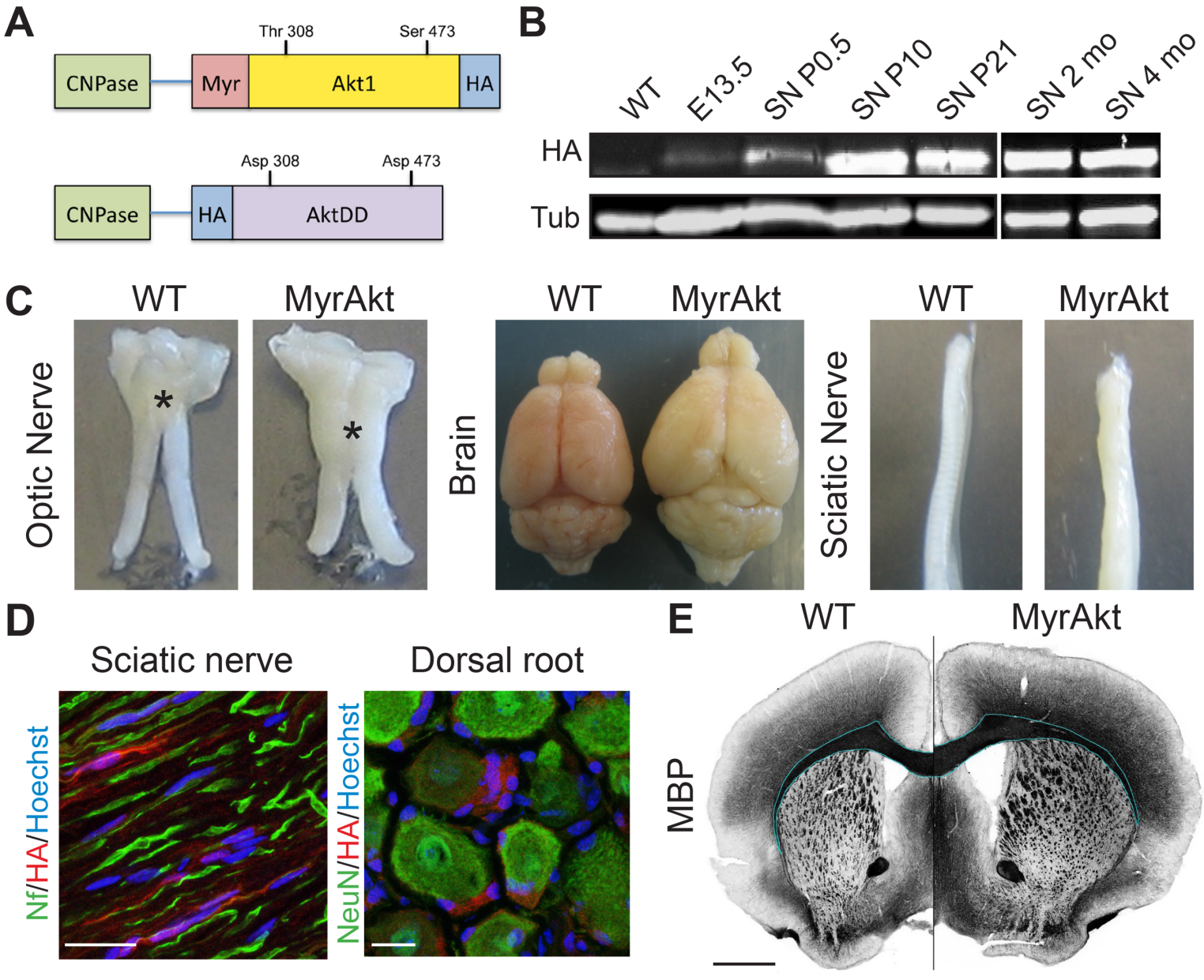
A
Thr 308
Ser 473
CNPase
Myr
Akt1
HA
Asp 308
Asp 473
CNPase
HA
AktDD
B
WT
E13.5
SN P0.5
SN P10
SN P21
SN 2 mo
SN 4 mo
HA
Tub
C
WT
MyrAkt
Optic Nerve
Brain
Sciatic Nerve
D
Sciatic nerve
Dorsal root
Nf/HA/Hoechst
NeuN/HA/Hoechst
E
WT
MyrAkt
MBP

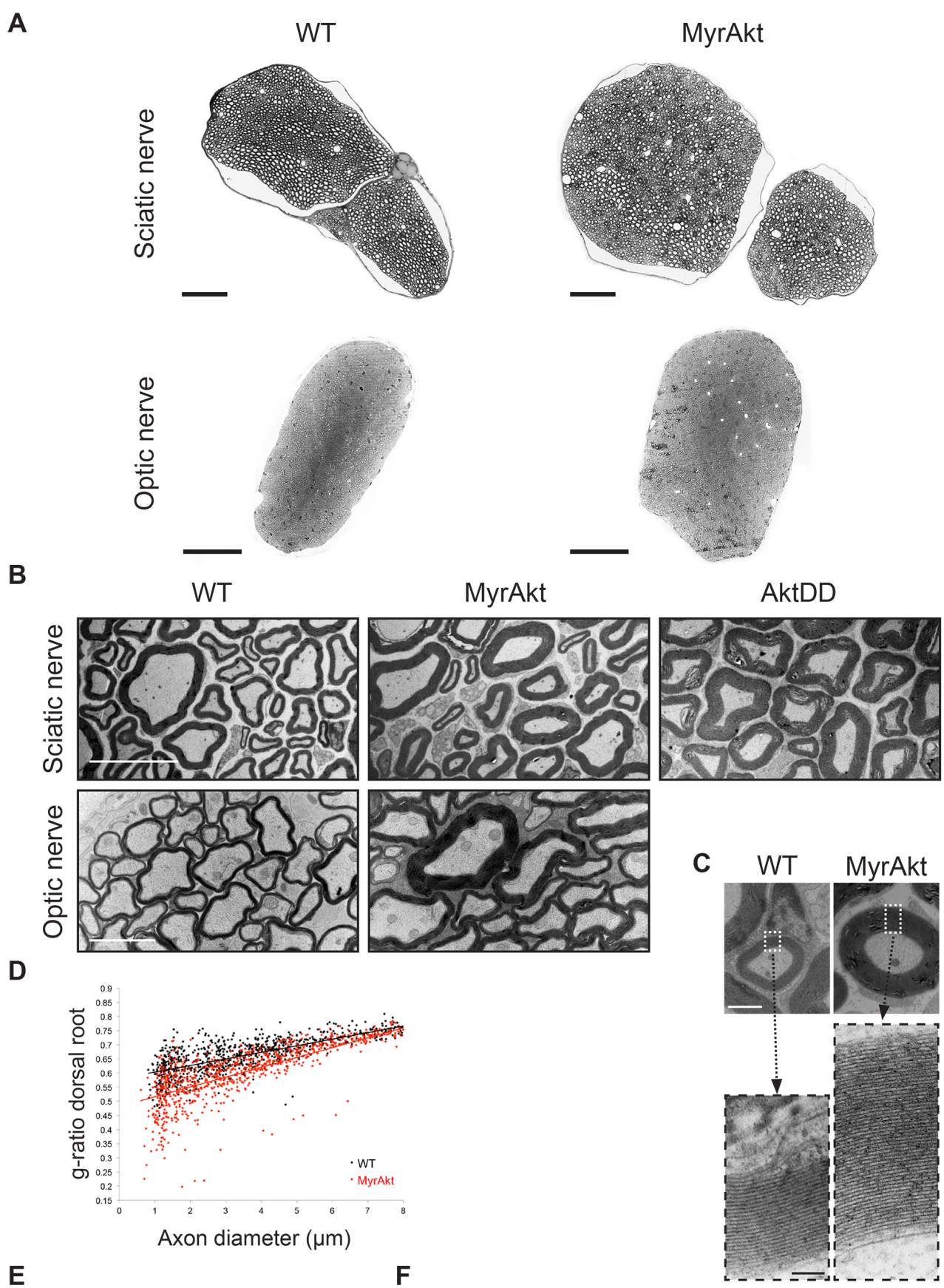
A
WT
MyrAkt
Sciatic nerve
Optic nerve
B
WT
MyrAkt
AktDD
Sciatic nerve
Optic nerve
C
WT
MyrAkt
D
g-ratio dorsal root
Axon diameter (μm)
WT
MyrAkt
E
g-ratio dorsal root
*
**
Total
Small
WT
MyrAkt
F
Hoechst positive
DR
VR
WT
MyrAkt

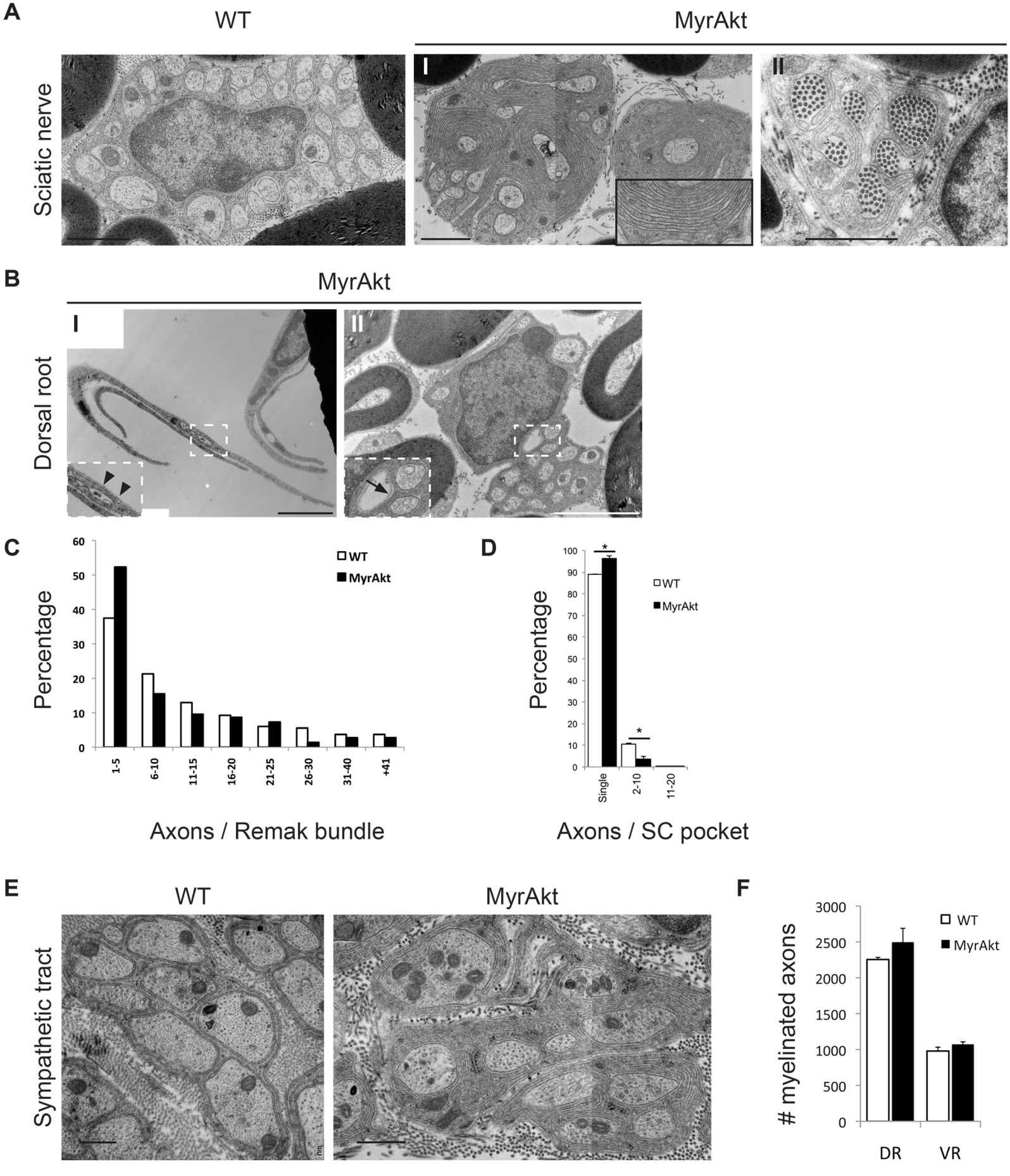
A
WT
MyrAkt
Sciatic nerve
I
II
B
MyrAkt
Dorsal root
I
II
C
Percentage
WT
MyrAkt
60
50
40
30
20
10
0
1-5
6-10
11-15
16-20
21-25
26-30
31-40
+41
Axons / Remak bundle
D
Percentage
WT
MyrAkt
100
90
80
70
60
50
40
30
20
10
0
*
*
Single
2-10
11-20
Axons / SC pocket
E
WT
MyrAkt
Sympathetic tract
F
myelinated axons
WT
MyrAkt
3000
2500
2000
1500
1000
500
0
DR
VR

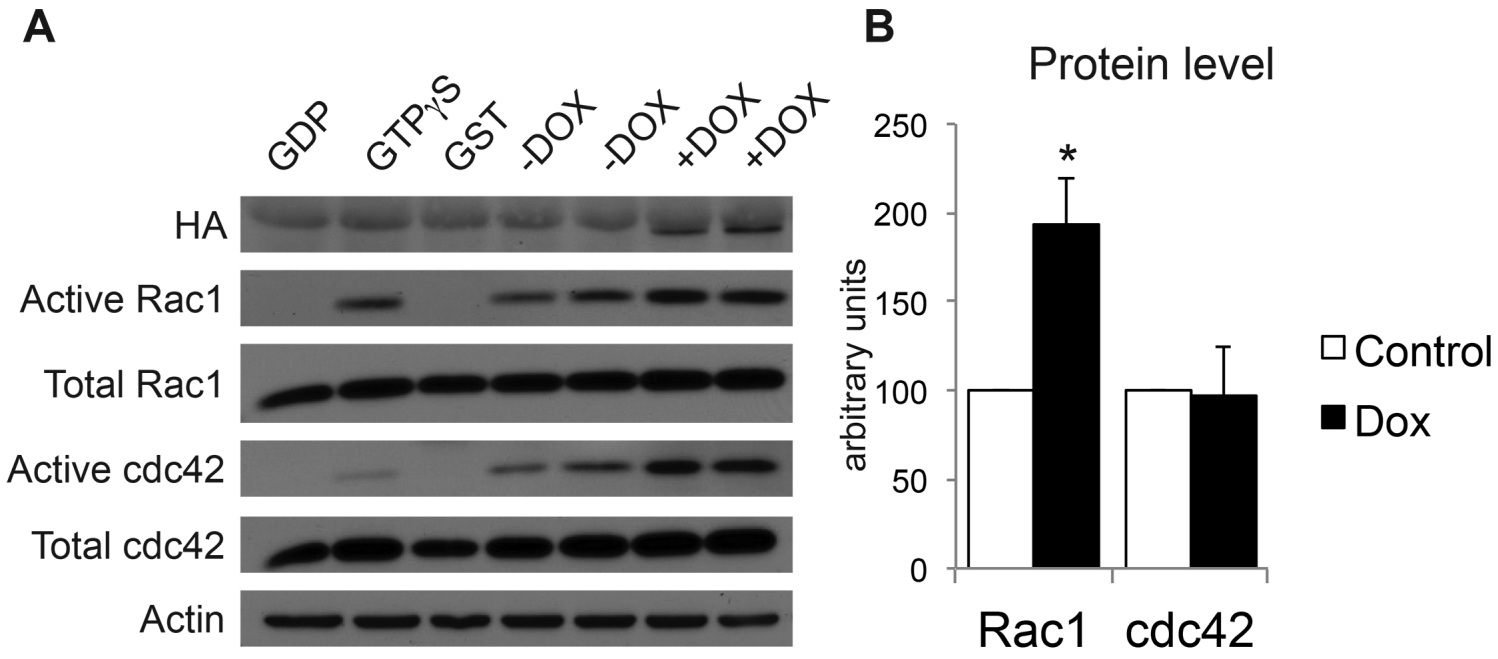
A
GDP
GTPγS
GST
-DOX
-DOX
+DOX
+DOX
HA
Active Rac1
Total Rac1
Active cdc42
Total cdc42
Actin
B
Protein level
250
200
150
100
50
0
arbitrary units
*
Rac1
cdc42
Control
Dox

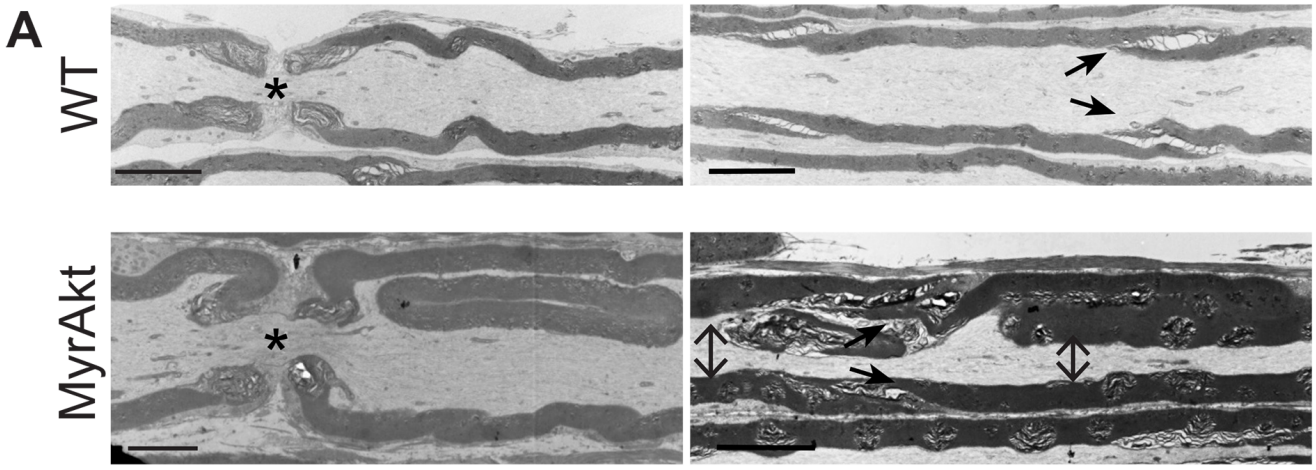
A
WT
MyrAkt

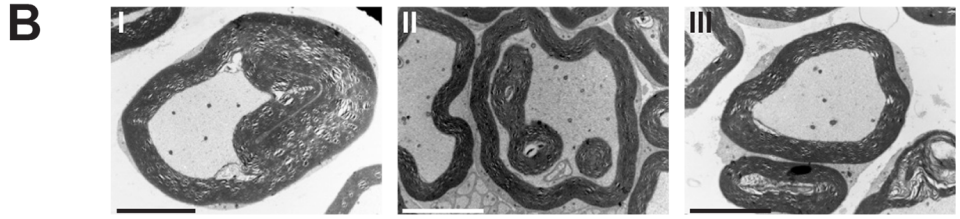
B
I
II
III

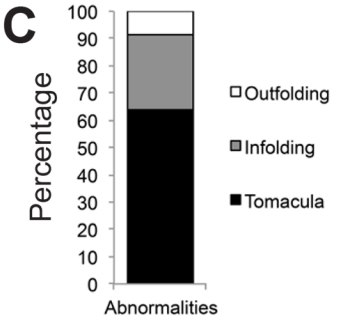
C
Percentage
100
90
80
70
60
50
40
30
20
10
0
Abnormalities
Outfolding
Infolding
Tomacula

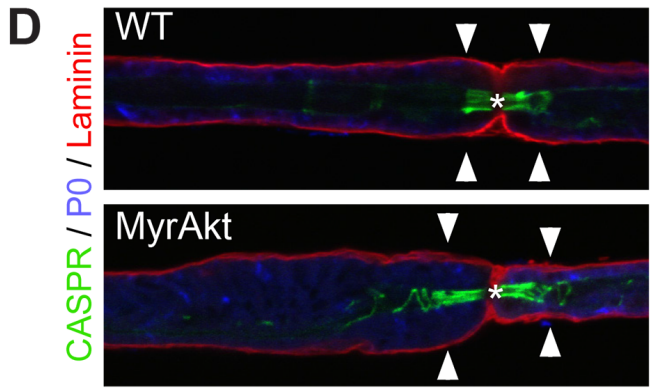
D
WT
MyrAkt
CASPR / P0 / Laminin

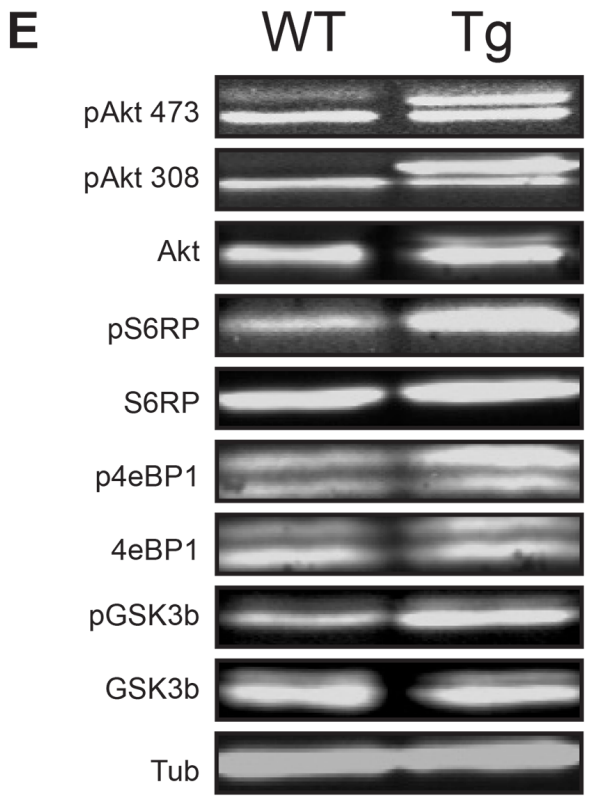
E
WT
Tg
pAkt 473
pAkt 308
Akt
pS6RP
S6RP
p4eBP1
4eBP1
pGSK3b
GSK3b
Tub

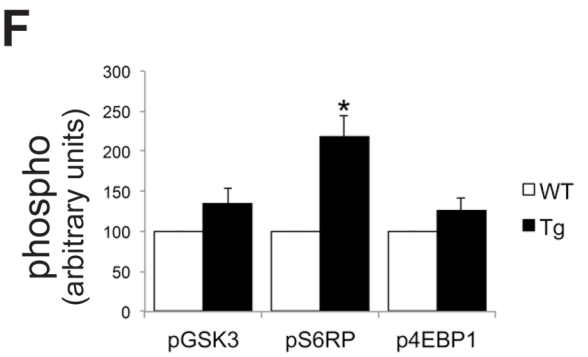
F
phospho
(arbitrary units)
300
250
200
150
100
50
0
pGSK3
pS6RP
p4EBP1
WT
Tg

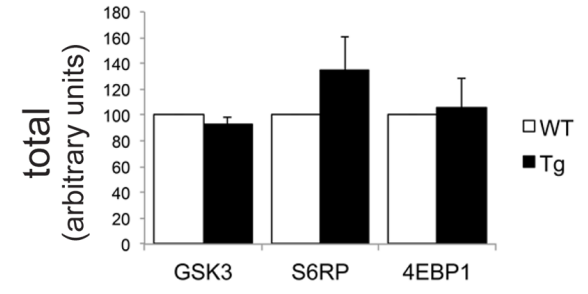
total
(arbitrary units)
180
160
140
120
100
80
60
40
20
0
GSK3
S6RP
4EBP1
WT
Tg

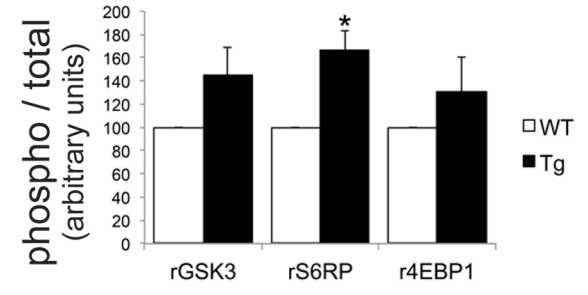
phospho / total
(arbitrary units)
200
180
160
140
120
100
80
60
40
20
0
rGSK3
rS6RP
r4EBP1
WT
Tg

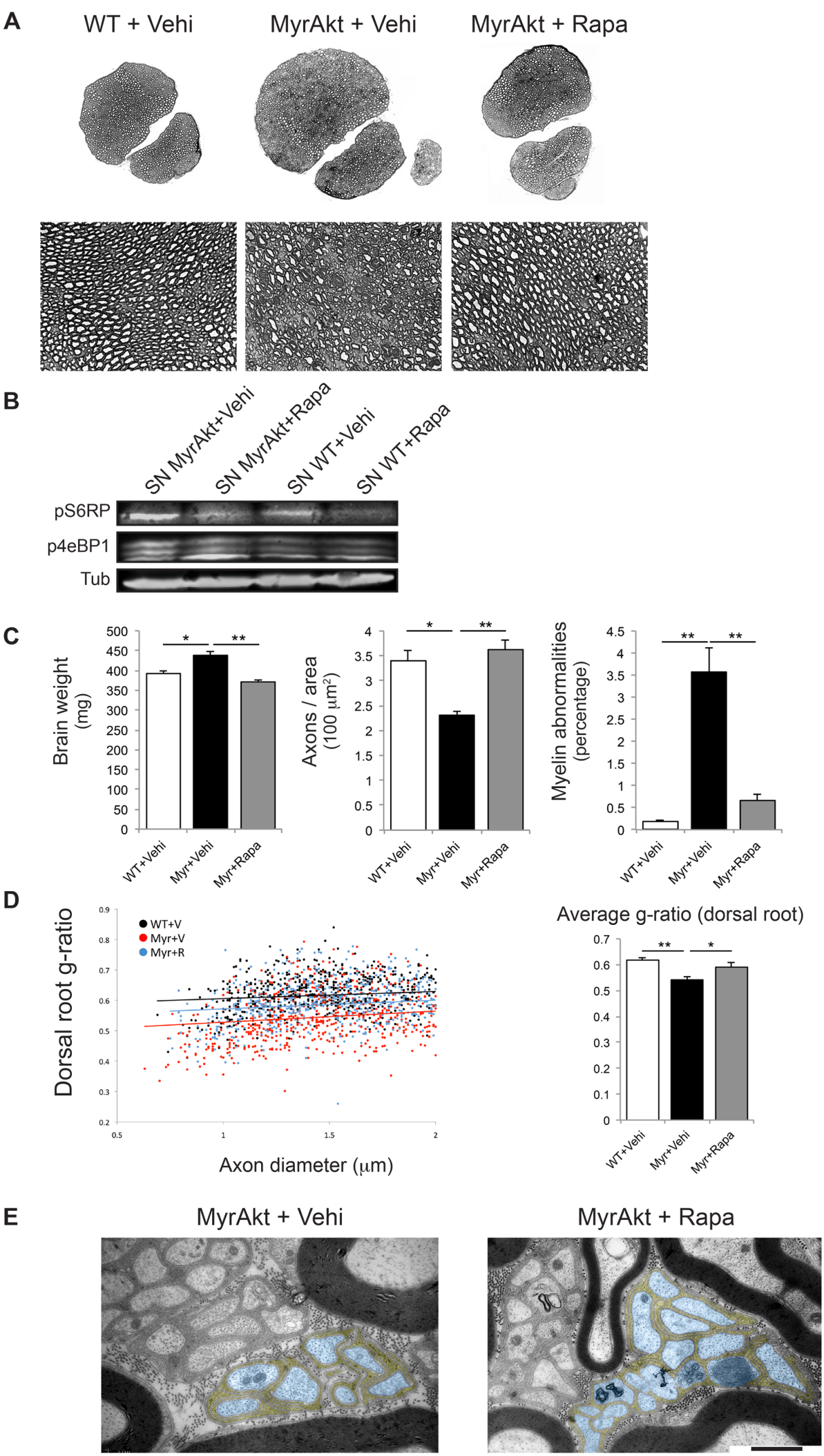
A
WT + Vehi
MyrAkt + Vehi
MyrAkt + Rapa
B
SN MyrAkt+Vehi
SN MyrAkt+Rapa
SN WT+Vehi
SN WT+Rapa
pS6RP
p4eBP1
Tub
C
Brain weight (mg)
Axons / area (100 μm²)
Myelin abnormalities (percentage)
WT+Vehi
Myr+Vehi
Myr+Rapa
D
Dorsal root g-ratio
WT+V
Myr+V
Myr+R
Axon diameter (μm)
Average g-ratio (dorsal root)
E
MyrAkt + Vehi
MyrAkt + Rapa